Article

Developmental Cell

Mutations in *ANKLE2*, a ZIKA Virus Target, Disrupt an Asymmetric Cell Division Pathway in *Drosophila* Neuroblasts to Cause Microcephaly

Graphical Abstract

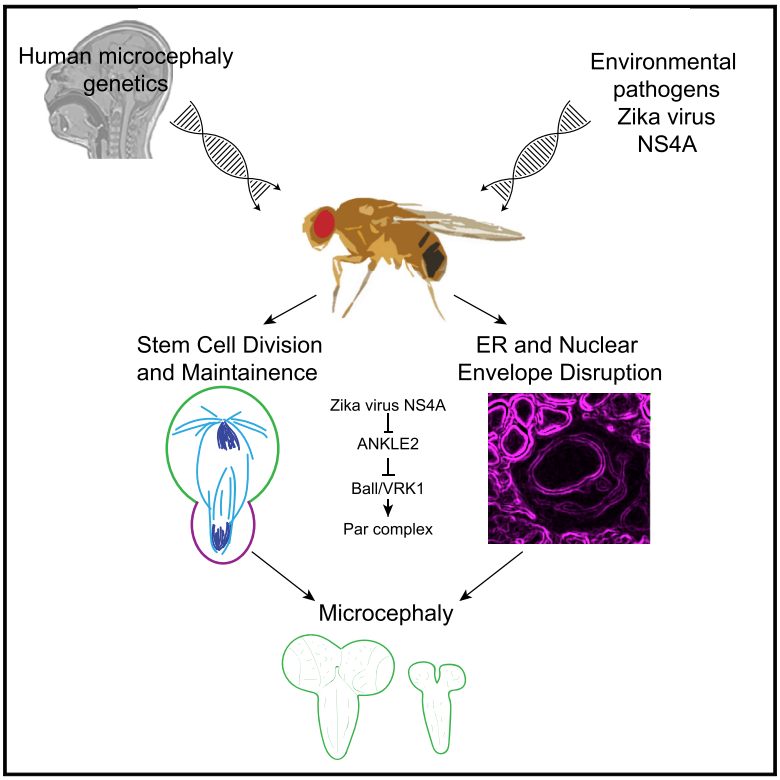

Authors

Nichole Link, Hyunglok Chung, Angad Jolly, ..., Ghayda M. Mirzaa, James R. Lupski, Hugo J. Bellen

Correspondence

hbellen@bcm.edu

In Brief

The Zika virus protein NS4A interacts with ANKLE2, a protein linked to hereditary microcephaly. Mutations in ANKLE2 also cause microcephaly-like phenotypes in flies. Link et al. now connect these phenotypes with disruption of an asymmetric cell division pathway in fly neuroblasts via an interaction between ANKLE2 and the kinase Ballchen-VRK1.

Highlights

- Ankle2 interacts with Ballchen/VRK1 to regulate brain development in *Drosophila*
- Ankle2/VRK1 pathway affects asymmetric protein localization during neuroblast division
- ANKLE2 and VRK1 are associated with human microcephaly
- The Zika virus protein NS4A interacts with and inhibits the ANKLE2 pathway

Link et al., 2019, Developmental Cell *51*, 713–729
December 16, 2019
https://doi.org/10.1016/j.devcel.2019.10.009

CellPress

Developmental Cell
Article

Mutations in *ANKLE2*, a ZIKA Virus Target, Disrupt an Asymmetric Cell Division Pathway in *Drosophila* Neuroblasts to Cause Microcephaly

Nichole Link,[1,2,3] Hyunglok Chung,[1,2,3] Angad Jolly,[2,4] Marjorie Withers,[2] Burak Tepe,[2,3,5] Benjamin R. Arenkiel,[2,3,5] Priya S. Shah,[6] Nevan J. Krogan,[7,8] Hatip Aydin,[9] Bilgen B. Geckinli,[10] Tulay Tos,[11] Sedat Isikay,[12] Beyhan Tuysuz,[13] Ganesh H. Mochida,[14,15,16] Ajay X. Thomas,[17,18] Robin D. Clark,[19] Ghayda M. Mirzaa,[20,21] James R. Lupski,[2,22,23,24] and Hugo J. Bellen[1,2,3,4,5,25,*]

[1]Howard Hughes Medical Institute, BCM, Houston, TX 77030, USA
[2]Department of Molecular and Human Genetics, BCM, Houston, TX 77030, USA
[3]Neurological Research Institute, Texas Children's Hospital, Houston, TX 77030, USA
[4]MD/PhD Medical Scientist Training Program and MHG Graduate program, BCM, Houston, TX 77030, USA
[5]Program in Developmental Biology, BCM, Houston, TX 77030, USA
[6]Department of Chemical Engineering and Department of Microbiology and Molecular Genetics, University of California, Davis, Davis, CA 95616, USA
[7]Department of Cellular and Molecular Pharmacology, University of California, San Francisco, San Francisco, CA 94158, USA
[8]California Institute for Quantitative Biosciences, QB3, University of California, San Francisco, San Francisco, CA 94158, USA
[9]Center of Genetics Diagnosis, Zeynep Kamil Maternity and Children's Training and Research Hospital, Istanbul, Turkey
[10]Department of Medical Genetics, Marmara University School of Medicine, Istanbul, Turkey
[11]Department of Medical Genetics, Dr. Sami Ulus Research and Training Hospital of Women's and Children's Health and Diseases, Ankara, Turkey
[12]Department of Physiotherapy and Rehabilitation, Hasan Kalyoncu University, School of Health Sciences, Gaziantep, Turkey
[13]Department of Pediatrics, Istanbul University-Cerrahpasa, Medical Faculty, Istanbul, Turkey
[14]Division of Genetics and Genomics, Department of Pediatrics and Manton Center for Orphan Disease Research, Boston Children's Hospital, Boston, MA 02115, USA
[15]Department of Pediatrics, Harvard Medical School, Boston, MA 02115, USA
[16]Pediatric Neurology Unit, Department of Neurology, Massachusetts General Hospital, Boston, MA 02114, USA
[17]Department of Pediatrics, Section of Neurology and Developmental Neuroscience, BCM, Houston, TX 77030, USA
[18]Section of Child Neurology, Texas Children's Hospital, Houston, TX 77030, USA
[19]Division of Medical Genetics, Department of Pediatrics, Loma Linda University Medical Center, Loma Linda, CA 92354, USA
[20]Department of Pediatrics, University of Washington, Seattle, WA 98195, USA
[21]Center for Integrative Brain Research, Seattle Children's Research Institute, Seattle, WA 98105, USA
[22]Department of Pediatrics, BCM, Houston, TX 77030, USA
[23]Texas Children's Hospital, Houston, TX 77030, USA
[24]Human Genome Sequencing Center, Baylor College of Medicine, Houston, TX 77030, USA
[25]Lead Contact
*Correspondence: hbellen@bcm.edu
https://doi.org/10.1016/j.devcel.2019.10.009

SUMMARY

The apical Par complex, which contains atypical protein kinase C (aPKC), Bazooka (Par-3), and Par-6, is required for establishing polarity during asymmetric division of neuroblasts in *Drosophila*, and its activity depends on L(2)gl. We show that loss of Ankle2, a protein associated with microcephaly in humans and known to interact with Zika protein NS4A, reduces brain volume in flies and impacts the function of the Par complex. Reducing Ankle2 levels disrupts endoplasmic reticulum (ER) and nuclear envelope morphology, releasing the kinase Ballchen-VRK1 into the cytosol. These defects are associated with reduced phosphorylation of aPKC, disruption of Par-complex localization, and spindle alignment defects. Importantly, removal of one copy of *ballchen* or *l(2)gl* suppresses *Ankle2* mutant phenotypes and restores viability and brain size. Human mutational studies implicate the above-mentioned genes in microcephaly and motor neuron disease. We suggest that NS4A, ANKLE2, VRK1, and LLGL1 define a pathway impinging on asymmetric determinants of neural stem cell division.

INTRODUCTION

Proper development of the human brain requires an exquisitely coordinated series of steps and is disrupted in disorders associated with congenital microcephaly. Congenital microcephaly in humans is characterized by reduced brain size (using occipital frontal circumference [OFC] as a surrogate measure) more than two standard deviations below the

mean (*Z* score < −2) at birth. It is associated with neurodevelopmental disorders such as developmental delay and intellectual disability and can be caused by external exposures to toxins, *in utero* infections, or gene mutations. Pathogenic gene variants for microcephaly have been identified through targeted genetic testing, genomic copy number studies, and exome sequencing (ES) (Brunetti-Pierri et al., 2008; Dumas et al., 2012; Lupski, 2015; Shinawi et al., 2010; Shaheen et al., 2019), identifying 18 primary microcephaly loci. Many syndromes significantly overlap with classic microcephaly phenotypes, and together, these disorders can be caused by defects in a wide variety of biological processes, including centriole biogenesis, DNA replication, DNA repair, cell cycle and cytokinesis, genome stability, and multiple cell signaling pathways (Jayaraman et al., 2018). In flies, we refer to microcephalic phenotypes when the third instar brain lobes are reduced in size (Yamamoto et al., 2014) or when adult flies exhibit small heads relative to the their body size (Oláhová et al., 2018). As in humans, microcephaly in flies can be a result of mutations that affect cell division and centrosome biology as demonstrated with mutations in WDR62 (Ramdas Nair et al., 2016; Lim et al., 2017) and ASPM or ASP (Rujano et al., 2013) but also those that affect the spindle assembly checkpoint (Poulton et al., 2017) and neuroblast (NB) proliferation (Kanai et al., 2018).

A forward, mosaic screen for neurodevelopmental and neurodegenerative phenotypes associated with lethal mutations on the X chromosome in *Drosophila* identified 165 loci, many with corresponding human genetic disease trait phenotypes (Yamamoto et al., 2014). Among them, a mutation in *Ankryin repeat and LEM domain containing 2* (*Ankle2*) causes loss of peripheral nervous system (PNS) organs in adult mutant clones and severely reduced brain size in hemizygous third instar larvae. To identify patients with pathogenic variants in *ANKLE2*, we surveyed the exome database of the Baylor-Hopkins Center for Mendelian Genomics (BHCMG) (Bamshad et al., 2012; Posey et al., 2019) and identified compound heterozygous mutations in *ANKLE2* in two siblings. Both infants exhibited severe microcephaly (*Z* score = −9), and the surviving patient displayed cognitive and neurological deficits alongside extensive intellectual and developmental disabilities. We showed that mutations in *Ankle2* led to cell loss of NBs and affected NB division in the developing third instar larval brain. Remarkably, expression of the wild-type human *ANKLE2* in flies rescued the observed mutant phenotypes (Yamamoto et al., 2014). Here, we explore the molecular pathways and proteins that are affected by *Ankle2* loss.

ANKLE2 belongs to a family of proteins containing LEM (LAP2, Emerin, and MAN1) domains that typically associate with the inner nuclear membrane (Lin et al., 2000; Barton et al., 2015). Conventional LEM proteins have been shown to interact with barrier to autointegration factor (BAF), which binds to both DNA and the nuclear lamina (Segura-Totten et al., 2002) to organize nuclear and chromatin structure. However, the LEM domain in *Drosophila* and *C. elegans* Ankle2 is not obviously conserved (Marchler-Bauer et al., 2017). Studies in *C. elegans* indicate that a homolog of ANKLE2 regulates nuclear envelope morphology and functions in mitosis to promote reassembly of the nuclear envelope upon mitotic exit (Asencio et al., 2012; Snyers et al., 2018). During this process, ANKLE2 modulates the activities of Vaccina-Related Kinase 1 (VRK1) and protein phosphatase 2A (PP2A) (Asencio et al., 2012). However, all experiments in worms were performed at the embryonic two-cell stage and no other phenotypes were reported except early lethality. While mutations in *ANKLE2* have been associated with severe microcephaly (OFC *Z* score = −2.5 to −9), human *VRK1* pathogenic variant alleles can cause a neurological disease trait consisting of complex motor and sensory axonal neuropathy and microcephaly (Gonzaga-Jauregui et al., 2013).

Mutations in both *Ankle2* and the fly homolog of *VRK1*, *ball-chen*, cause a loss of NBs in 3rd instar larval brains in *Drosophila* (Yamamoto et al., 2014; Yakulov et al., 2014). NBs divide asymmetrically and are often used as a model to investigate stem cell biology (Homem and Knoblich, 2012) and asymmetric cell division (Gallaud et al., 2017). Most NBs in the larval central brain give rise to another NB and a smaller ganglion mother cell (GMC), which then divides once again to produce neurons or glia. Proper NB maintenance and regulation is essential for precise development of the adult nervous system, and misregulation of NB number or function can lead to defects in brain size (Wang et al., 2009; Gateff and Schneiderman, 1974).

Congenital Zika virus infection in humans during pregnancy has been associated with severe microcephaly that can be as dramatic as certain genetic forms of microcephaly including phenotypes associated with biallelic mutations in MCPH16/*ANKLE2* (Moore et al., 2017; Yamamoto et al., 2014). Recently, we showed that a Zika virus protein, NS4A, physically interacts with ANKLE2 in human cells. Expression of NS4A in larval brains causes microcephaly, induces apoptosis, and reduces proliferation. Importantly, expression of human ANKLE2 in flies that express NS4A suppresses the associated phenotypes, demonstrating that NS4A interacts with the ANKLE2 protein and inhibits its function (Shah et al., 2018). Interestingly, Zika virus crosses the blood brain barrier and targets radial glial cells, the neural progenitors in the vertebrate cortex (Devhare et al., 2017; Tang et al., 2016).

Here, we show that Ankle2 is localized to the endoplasmic reticulum and nuclear envelope, similar to NS4A, and genetically interacts with *ball-VRK1* to regulate brain size in flies. An allelic series at the *ANKLE2* and *VRK1* loci shows that perturbation of this pathway results in neurological disease including microcephaly. Our data indicate that the Ankle2-Ball (VRK1) pathway is required for proper localization of asymmetric proteins and spindle alignment during NB cell division by affecting two proteins, atypical protein kinase C (aPKC) and L(2)gl, which play critical roles in the asymmetric segregation of cell fate determinants. In addition, NS4A expression in NBs mimics phenotypes seen in *Ankle2* mutants, and NS4A induced microcephaly is suppressed by removing a single copy of *ball* or *l(2)gl*. Human genomics variant data and disease trait correlations extend this asymmetric cell division pathway from proteins identified in flies and reveal insights into neurological disease. In summary, NS4A hijacks the Ankle2-Ball (VRK1) pathway, which regulates progenitor stem cell asymmetric division during brain development and defines a human microcephaly pathway.

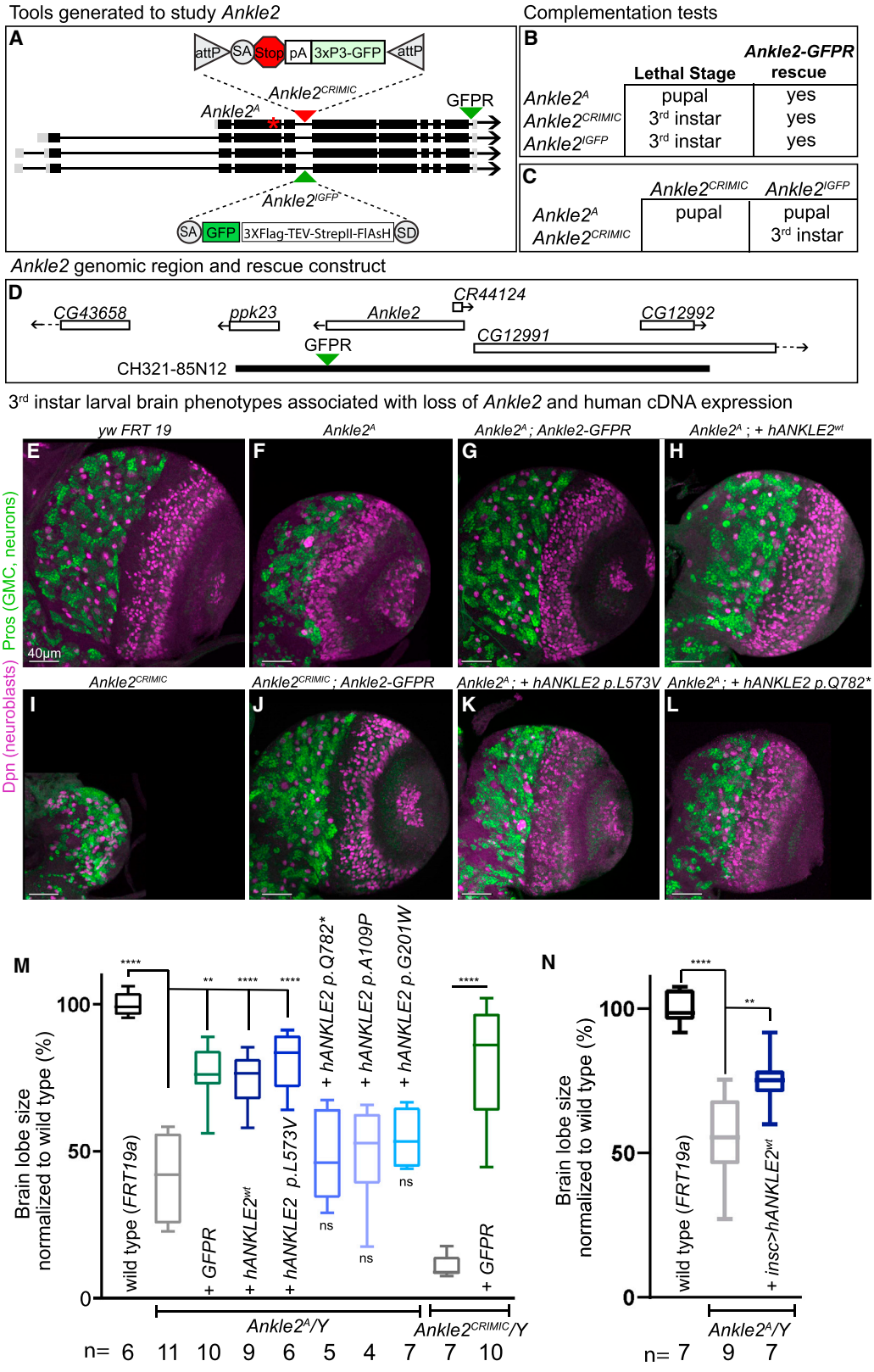

Figure 1. Mutations in *ANKLE2* Cause Microcephaly in Humans and *Drosophila*

The structure and transcripts of the *Ankle2* gene with insertional mutations or tags are shown in (A). *Ankle2*^{A}, noted by *, is an EMS generated L326H mutation, while *Ankle2*^{CRIMIC} represents a CRISPR-Cas9-mediated MIMiC-like (CRIMIC) insertion in the 4th coding intron (Lee et al., 2018). ΦC31-mediated cassette

(legend continued on next page)

RESULTS

Human ANKLE2 Variants Cause Microcephaly

We previously reported that compound heterozygous variants in *ANKLE2* are associated with microcephaly (*Z* score = −9) (MCPH16, MIM#616681) in two affected siblings (Yamamoto et al., 2014). Here, we report two additional probands carrying unique variants in *ANKLE2* identified in Seattle (LR17-511 and LR18-033; Figures S1 and S2; Table S1). Brain MRIs of an age-matched control (Figure S1A) and a proband with microcephaly from family LR17-511 document one of the more severe cases of microcephaly (*Z* score = −8) (Figure S1B). To investigate potential genotype-phenotype correlations, we explored the spectrum of reported neurological disease trait manifestations associated with *ANKLE2* present in the Baylor Genetics (BG) Laboratories databases. These contain results of clinical exome sequencing of patients with presumed genetic disorders that remain unsolved for a molecular diagnosis but patients or families have consented to research analyses. We screened for rare biallelic variants, predicted damaging, in *ANKLE2* that fulfill Mendelian expectations for a recessive disease trait. Three families were found to fulfill these criteria in probands with neurologically associated phenotypes (Figures S1D and S2; Table S2). These cases suggest that a diverse set of variants in *ANKLE2* may be associated with a spectrum of neurologic diseases and reveal either sporadic disease, apparent vertical transmission, and in some cases, consanguineous parentage (Yamamoto et al., 2014; Shaheen et al., 2019). The identified mutations are missense, nonsense, or splicing variants that lead to premature stop codons; all subjects have biallelic variants, either compound heterozygous or homozygous alleles (Figures S1 and S2). Probands exhibit congenital microcephaly but some also present with severe brain MRI abnormalities and skin pigmentation abnormalities (Figure S1D). These aggregate data demonstrate that mutations in *ANKLE2* cause autosomal recessive microcephaly.

Null Alleles of *Ankle2* Are Associated with Reduced Brain Size in Flies

Given the human genetic implications noted above, we used *Drosophila* to elucidate molecular mechanisms underlying *ANKLE2*-associated microcephaly. The mutation originally identified in flies, $Ankle2^{A}$ (L326H), causes reduced brain size in third instar larvae and leads to pupal lethality at temperatures $\geq 22^{\circ}C$ (Figure S3A). It results in decreased NB number, reduced cell divisions when assessed in MARCM clones, and a high incidence of apoptotic cell death throughout the brain, including NBs and neurons (Yamamoto et al., 2014). However, first instar larvae are born with a slight, but not significant, reduction in the number of NBs or Dpn-positive cells (Figures S3B and S3C) indicating that *Ankle2* loss causes a premature differentiation, loss of stem cell markers, or death of NBs.

To create a severe loss-of-function allele for *Ankle2*, we integrated a CRISPR-Cas9-mediated MIMiC-like (CRIMIC) construct containing *attP-FRT-SA-3XSTOP-polyA-3xP3-EGFP-FRT-attP* sequences using CRISPR-Cas9 in the fifth intron shared by all isoforms (Figure 1A, pM14; Lee et al., 2018). The construct leads to a truncated transcript that likely corresponds to a null allele ($Ankle2^{CRIMIC}$, Figure 1A). These animals die as 3rd instar larvae (Figure 1B), are smaller than wild-type and $Ankle2^{A}$ animals, and show a very severely reduced brain volume (Figure 1E versus Figures 1I and 1M) with complete disruption of brain morphology, especially the optic lobe (Figure 1I). Since the severe phenotypes make it difficult to assess the biological questions presented below, we assayed the majority of phenotypes with the hypomorphic $Ankle2^{A}$ missense allele.

To determine whether *Ankle2* is expressed in the brain, we used the CRIMIC allele to introduce an artificial exon that contains SA-GFP-SD in frame, which produces a tagged fusion protein ($Ankle2^{IGFP}$, Figures 1A and 1B) (Lee et al., 2018). We readily detect $Ankle2^{IGFP}$ protein in brains of heterozygous animals (Figure S4A). However, homozygous animals are lethal and exhibit very small brains, indicating that integration of this exon disrupts protein function. Based on complementation tests, the strength of the allelic series is $Ankle2^{A} < Ankle2^{CRIMIC} = Ankle2^{IGFP}$ (Figures 1B and 1C). We therefore used recombineering (Venken et al., 2006) to add a C-terminal GFP tag to Ankle2 in a bacterial artificial chromosome (BAC CH321-85N12; referred to as *Ankle2-GFPR*, Figures 1A and 1D) (Venken et al., 2008, 2009). When this P[acman] clone was introduced in all three *Ankle2* mutant backgrounds, *Ankle2-GFPR* rescued brain phenotypes and lethality of these alleles (Figures 1B, 1G, and 1J). Hence, the chromosomes carrying the three *Ankle2* alleles do not carry second-site mutations that affect brain size or viability, and the tagged protein is likely to reflect the endogenous Ankle2 protein distribution.

The human reference *ANKLE2* gene rescues lethality and small brain phenotypes of $Ankle2^{A}$ animals when expressed

exchange replaced the stop-polyA in $Ankle2^{CRIMIC}$ with an artificial exon cassette consisting of SA-GFP-SD (Venken et al., 2011) to produce $Ankle2^{IGFP}$. A C-terminal GFP-tagged *Ankle2* genomic rescue construct (Ankle2-GFPR) was generated using recombineering (Venken et al., 2008). (B) Lethal stages and rescue by Ankle2-GFPR or (C) complementation tests of $Ankle2^{A}$, $Ankle2^{CRIMIC}$, and $Ankle2^{IGFP}$. (D) *Ankle2* gene structure and genomic rescue construct (CH321-85N12) (Venken et al., 2009). (E–L) Partial projections of 3rd instar larval brains stained with Deadpan (Dpn) (purple, neuroblasts) a neuroblast marker (Bier et al., 1992) and Pros (green, GMC, neurons) a neuronal lineage marker (Campbell et al., 1994) to document overall brain structure are shown in (E) wild-type (*y w FRT19a*), (F) *y w* $Ankle2^{A}$ *FRT19a*, (G) *y w* $Ankle2^{A}$ *FRT19a; Ankle2-GFPR*, (H) *y w* $Ankle2^{A}$ *FRT19a; da::hANKLE2*^{wt}, (I) $Ankle2^{CRIMIC}$, (J) $Ankle2^{CRIMIC}$*; Ankle2-GFPR*, (K) *y w* $Ankle2^{A}$ *FRT19a; da:: hANKLE2 p.L573V*, and (L) *y w* $Ankle2^{A}$ *FRT19a; da:: hANKLE2 p.Q782** animals. The C-terminal GFP-tagged rescue P[acman] clone CH321-85N12, (*Ankle2-GFPR*, diagramed in [A] and [B]) rescues brain morphology, brain size, and lethality in both *y w* $Ankle2^{A}$ *FRT19a* (G) and $Ankle2^{CRIMIC}$ (J) animals. Scale bars = 40μm. Images were cropped using Photoshop to isolate a single lobe from each brain and placed in front of black backgrounds for figure presentation. Quantification of brain size is shown in (M). Box plot hinges represent the 25th to 75th percentiles, the central line is the median, and whiskers represent minimum to maximum. Note that hANKLE2^{wt} and hANKLE2 p.L573V rescue brain size and lethality of $Ankle2^{A}$ mutants, whereas hANKLE2 p.Q782*, hANKLE2 p.A109P, and hANKLE2 p.G201W do not. Here, Ankle2-GFPR is reported as GFPR. (N) Neuroblast-specific expression of wild-type human ANKLE2 (*y w* $Ankle2^{A}$ *FRT19a; insc::hANKLE2*^{wt}) partially rescues brain size of $Ankle2^{A}$ mutants. For quantifications, the total number counted (n) is noted below each graph. One-way ANOVA with multi-comparison post-test. **p < 0.01, ****p < 0.0001.
See also Figures S1–S3.

Ankle2 localizes with ER markers and is required for proper ER morphology

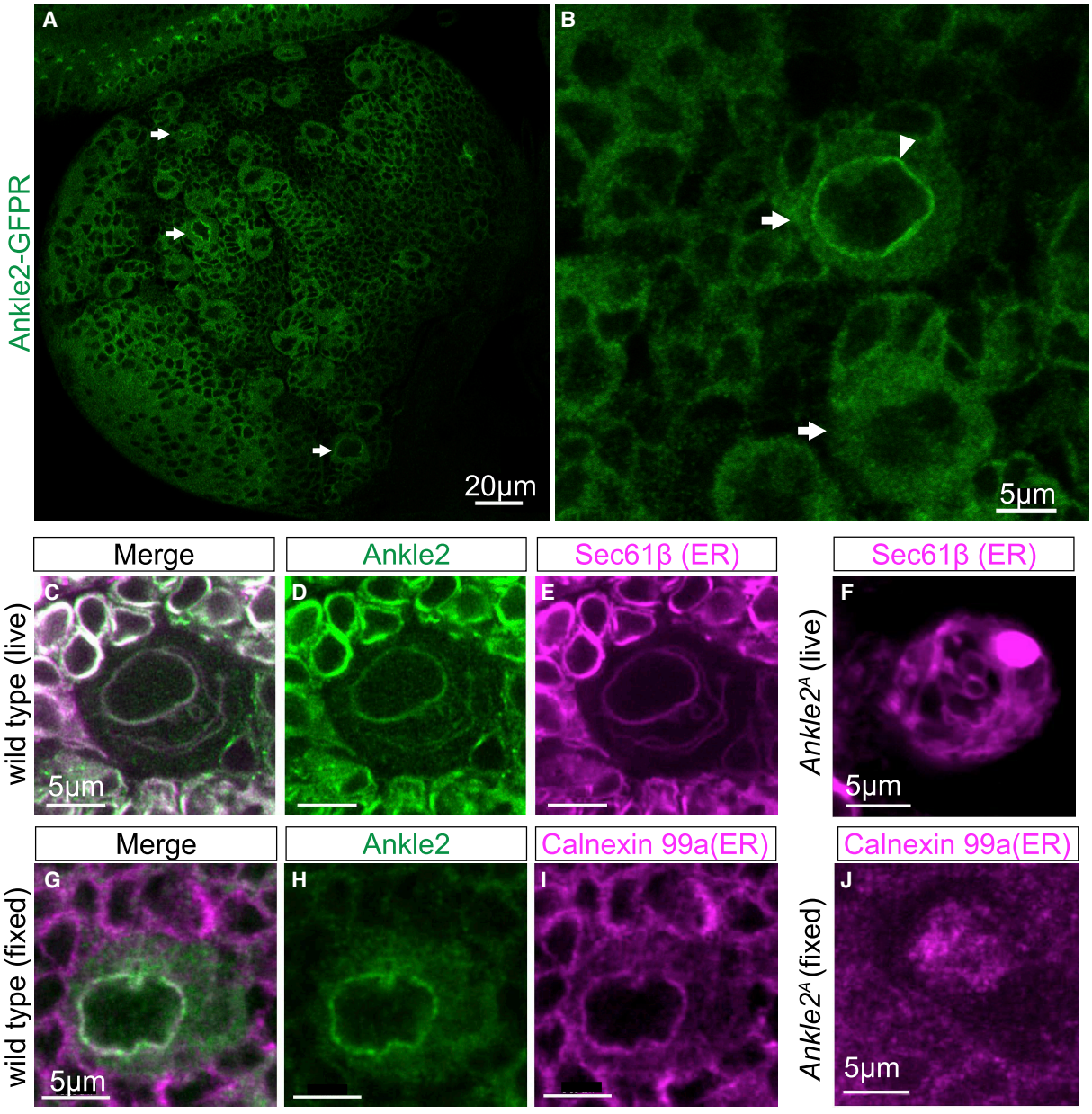

Ankle2 localizes with the nuclear envelope and is required for its morphology

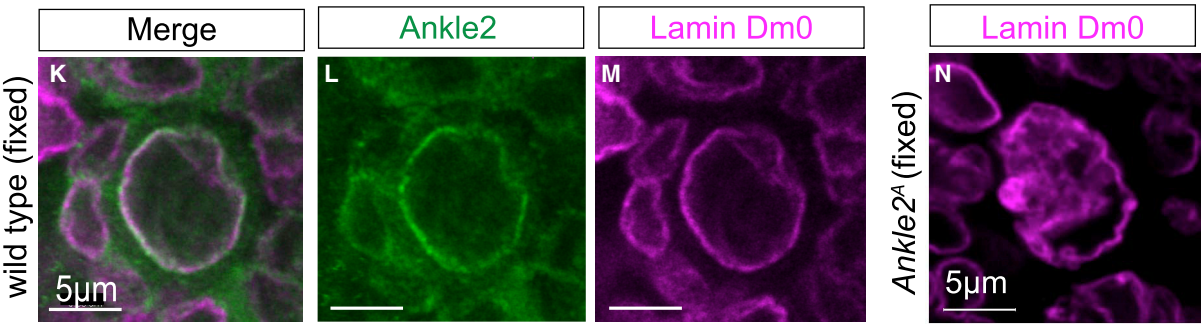

(legend on next page)

ubiquitously (*da-GAL4>UAS-hANKLE2*, Figures 1H and 1M) or in NBs only (*insc-GAL4>UAS-hANKLE2*, Figure 1N). To determine whether the microcephaly-associated mutations in human ANKLE2 are loss-of-function alleles, we next expressed *ANKLE2 p.L573V*, *ANKLE2 p.Q782**, *ANKLE2 p.A109P*, *ANKLE2 p.G201W*, in *Ankle2*^{A} mutant animals. The p.Q782*, p.A109P, and p.G201W variants failed to rescue lethality or reduced brain sizes (Figures 1L and 1M) consistent with them being severe loss-of-function variant alleles. However, p.L573V restored both viability and brain size (Figures 1K and 1M) in some *Ankle2*^{A} animals (Figure 1M), suggesting that this variant is a mild hypomorphic allele.

Ankle2 Localizes to the Endoplasmic Reticulum and Nuclear Envelope and Is Required for Their Integrity

The endogenously tagged Ankle2^{IGFP} (Figure S4A) as well as the tagged genomic rescue (GR) construct *Ankle2-GFPR* (Figures 2A, 2B, and S4B–S4G) show that *Ankle2* is expressed in most tissues including larval disks (Figures S4B and S4C), embryos (Figures S4D–S4F), and cells of the third instar larval brain. NBs, GMCs, and neurons (Figure S4G) all show high expression of Ankle2. The protein appears to be localized to the cytoplasm of all cells including NBs (arrows in Figures 2A and 2B). However, in a subset of cells, the protein is clearly enriched at the nuclear envelope (arrowhead). To determine the dynamics of Ankle2 protein localization, we performed live imaging. As shown in Video S1, the protein is recruited to the nuclear envelope at the initiation of mitosis and remains associated with the nuclear envelope until briefly after cytokinesis. Indeed, Ankle2 is enhanced at the nuclear envelope in cells positive for phospho-histone H3 (pHH3), a mitotic marker (Figures S4H and S4I, arrowhead). Hence, Ankle2 is localized to the nuclear envelope in NBs undergoing mitosis.

To determine precisely where Ankle2 is localized, we performed live imaging of brains from animals carrying *Ankle2-GFPR* and a transgene that labels the endoplasmic reticulum (ER): *da-Gal4>UAS-Sec61β-tdTomato* (Summerville et al., 2016). In NBs (large cell in Figures 2C–2E), the Ankle2 protein fully colocalizes with Sec61β at the nuclear envelope as well as the ER. In the surrounding neurons (small cells), much of the cytoplasm is co-labeled. We also counter-stained fixed samples with Calnexin 99a, another ER marker (Riedel et al., 2016). Again, Ankle2 localizes to the nuclear envelope and the ER, but in fixed samples, the ER structure is less obvious than in live imaging (Figures 2G–2I).

To determine if Ankle2 is required for proper ER structure, we performed live imaging of *Ankle2*^{A} mutant NBs expressing Sec61β-tdTomato (Figure 2F). When compared to wild-type (Figure 2E), *Ankle2*^{A} mutants display highly aberrant Sec61β localization in many NBs (25°C). The NB in Figure 2F appears larger than normal and displays Sec61β folds within the nucleus. In addition, we stained fixed *Ankle2*^{A} mutant NBs with Calnexin 99a and found that *Ankle2*^{A} mutants also display irregular Calnexin 99a localization (Figure 2J versus Figure 2I), similar to defects shown in Figure 2F, suggesting that even a partial loss of Ankle2 disrupts the ER and possibly the nuclear envelope structure. Indeed, the morphology of the nuclear envelope is aberrant and convoluted in some *Ankle2*^{A} mutant cells when stained with lamin Dm0 (Riemer et al., 1995), a nuclear envelope marker (compare Figure 2N with Figures 2K–2M). Hence, Ankle2 is required for proper ER and nuclear envelope morphology.

Ankle2 Mutations Affect the Asymmetric Localization of NB Determinants

Because of the reduced cell proliferation and reduced NB number in *Ankle2*^{A} third instar brains (Yamamoto et al., 2014), we sought to explore NB division in more detail. NB polarity during division relies on the function of the highly conserved apically localized partitioning defective (Par) complex, which consists of Bazooka (Baz, Par-3) (Schober et al., 1999), Par-6 (Petronczki and Knoblich, 2001), and aPKC (Rolls et al., 2003). Once activated, the Par complex is responsible for restricting Miranda (Mira) and other cell fate determinants to the basal domain of NBs. After division in most NBs, the basal domain will become the GMC, which divides again to produce neurons or glia (Betschinger et al., 2003; Atwood and Prehoda, 2009). Several proteins have been implicated in regulating the Par complex (Chabu and Doe, 2009; Andersen et al., 2012; Bonaccorsi et al., 2007; Atwood et al., 2007), including those associated with cell cycle regulation (Chabu and Doe, 2008; Lee et al., 2006; Wang et al., 2006, 2007).

A previous inspection of dividing NBs revealed no obvious defects in Mira staining (Yamamoto et al., 2014). However, a quantitative analysis of dividing *Ankle2*^{A} NBs stained with anti-Baz, Par-6, aPKC, and Mira revealed severe localization defects of these proteins in greater than 40% of metaphase NBs during asymmetric division (Figures 3A–3L, quantified in Figures 3M–3P) in both *Ankle2*^{A} and transheterozygous animals (*Ankle2*^{A}/*Ankle2*^{CRIMIC}). These defects are rescued by the genomic construct (Figure 1D), *Ankle2-GFPR* (Figures 3D, 3H, 3L, and 3M–3P). Finally, we performed live imaging of 3rd instar larval brains of wild-type (Video S2) and *Ankle2*^{A} mutants labeled with Mira-Red Fluorescent Protein (RFP) and Histone-GFP (Videos S3, S4, and S5). As shown in Videos S3, S4, and S5, NBs exhibit abnormal Mira localization as well as instances of

Figure 2. Ankle2 Localizes to the ER and Is Dynamically Expressed in the Brain

(A and B) 3rd instar larval brains from *Ankle2-GFPR* animals stained for GFP to document Ankle2 expression and localization in (A) and (B) single slices (arrows point to neuroblasts). (A) Scale bar = 20μm. (B) Scale bar = 5μm.

(C–E) Live imaging of Ankle2 (D, green) and the ER labeled with Sec61B ([E], *da-GAL4*, *UAS*-Sec61β-tdTomato, purple) (Summerville et al., 2016) shows strong colocalization.

(F) Live *Ankle2*^{A} mutant neuroblast displays aberrant Sec61β-tdTomato expression.

(G–I) Fixed *Ankle2-GFPR* animals highlighting Ankle2-GFP (green) and another ER marker (calnexin 99a, purple) (Riedel et al., 2016).

(J) Fixed *Ankle2* mutant animals (*Ankle2*^{A}) display aberrant ER structures (Calnexin 99a, purple).

(K–M) Ankle2 (L, green) colocalizes with some portions of the nuclear envelope (Lamin Dm0, purple).

(N) *Ankle2* mutant animals (*Ankle2*^{A}) display a disrupted nuclear envelope structure (Lamin Dm0, purple). Scale bars in (C–N) = 5 μm.

See also Figure S4 and Video S1.

Ankle2 is required for asymmetric protein localization

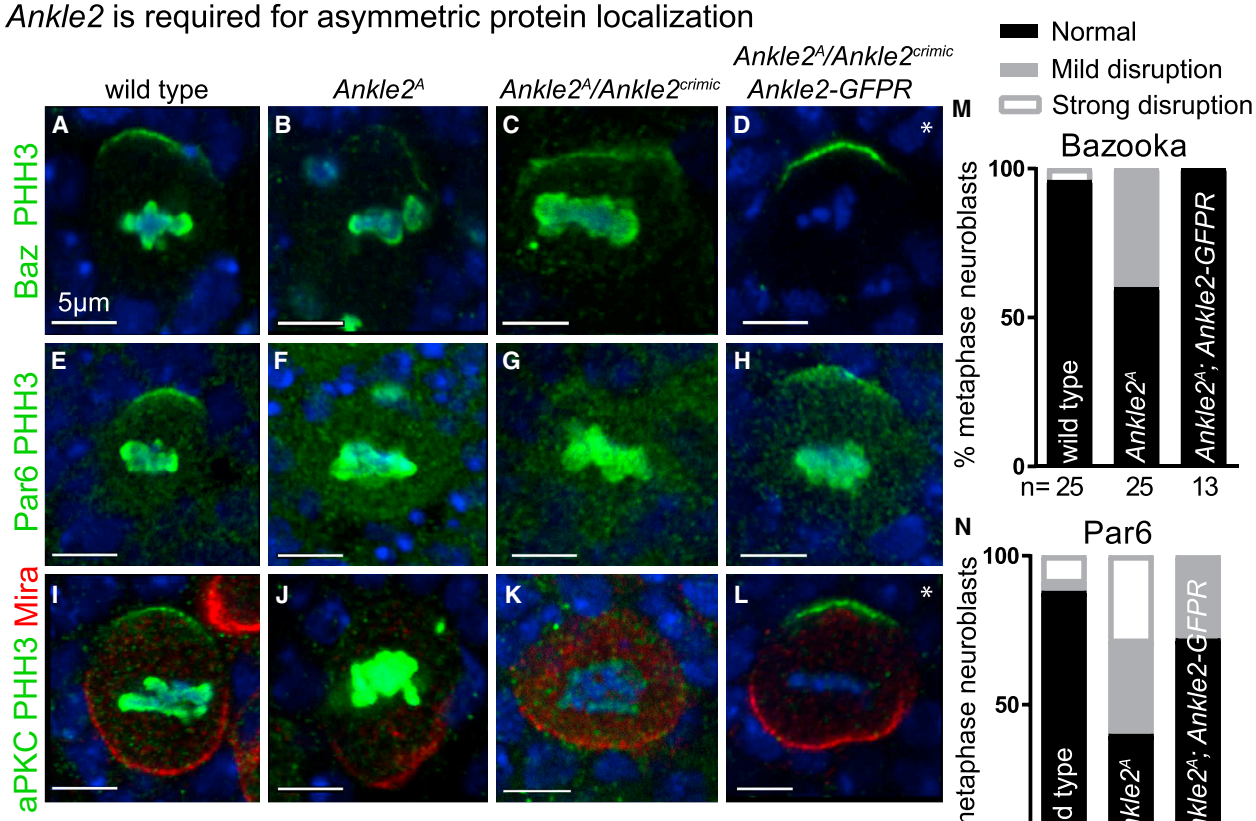

Ankle2 is required for spindle alignment and centrosome number

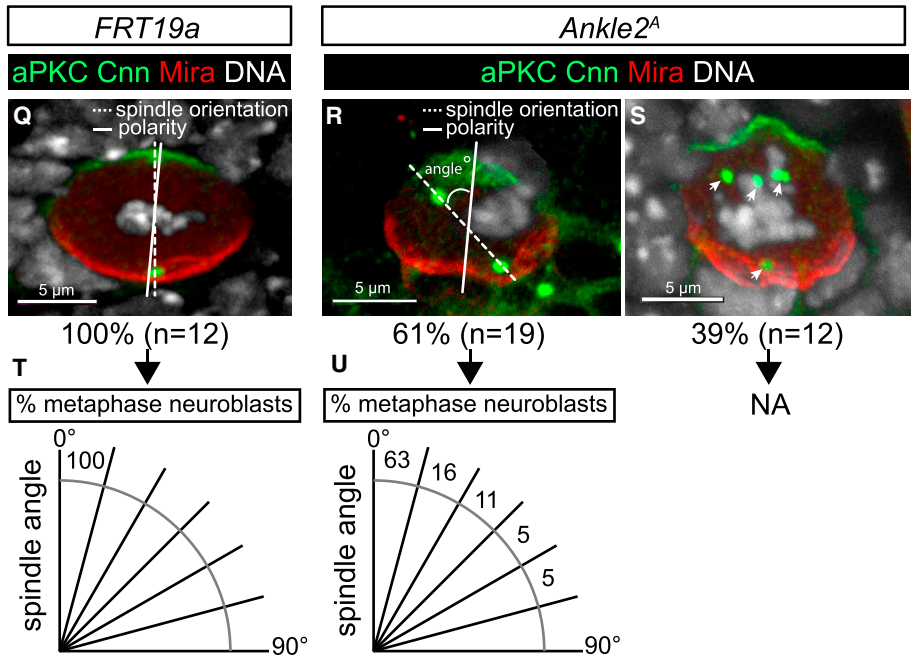

(legend on next page)

failed division including DNA segregation defects, chromatin bridges, and cytokinesis defects (Videos S3 and S4).

For proper NB division to occur, cells must not only asymmetrically localize Par-complex members and cell fate determinants, they must also align the mitotic spindle so that divisions segregate cell fate determinants to the proper daughter cell (Cabernard and Doe, 2009). In wild-type NBs, the mitotic spindle is aligned parallel to the polarity axis (Figures 3Q and 3T). Our initial observations in *Ankle2*^{A} mutants suggested no defects in mitotic spindle alignment in many cells (Yamamoto et al., 2014), but after a quantitative analysis of metaphase NBs, we noted that spindle alignment appeared disrupted in some *Ankle2*^{A} mutant cells. To quantify these defects, we measured the axis of division using DNA and centrosomin (Cnn) (Lucas and Raff, 2007) to highlight centrosome placement relative to the localization of cell polarity proteins aPKC and Mira (Figures 3Q–3U). Surprisingly, we found that nearly 40% of *Ankle2*^{A} mutant NBs contained supernumerary centrosomes (Figure 3S). In the remaining 60% of *Ankle2*^{A} mutant metaphase NBs with obvious aPKC or Mira localization, we also found varying degrees of mitotic spindle alignment defects (compare Figures 3Q, 3R, 3T, and 3U), showing that Ankle2 is also required for proper spindle alignment in NB division. Together, these results show that Ankle2 plays a prominent role in asymmetric protein localization, spindle alignment, and cell division of NBs.

Ankle2 Interacts with VRK1-Ballchen

A *C. elegans* homolog of Ankle2, Lem4L, was previously shown to physically and genetically interact with VRK1, the homolog of Ballchen (Ball) in flies (Asencio et al., 2012). Lem4L and VRK1 in worms localize to the nuclear envelope of the 2-cell stage embryo (Asencio et al., 2012). In contrast, Ball appears to be nuclear during interphase and prophase in all *Drosophila* cells (Figure S3D) (Yakulov et al., 2014) as well as in mammalian cells (Figures 4G and 4H), and both fly and human proteins have nuclear localization signals. Interestingly, human *VRK1* pathogenic variants cause reduced brain size and microcephaly as well as axonal neuropathy in affected patients (Gonzaga-Jauregui et al., 2013; Renbaum et al., 2009). Hence, to characterize the relationship between Ankle2 and Ball-VRK1, we analyzed the expression and localization of Ball and Ankle2 during NB cell division (Figures 4A–4D). During interphase, Ankle2 and Ball do not colocalize as Ankle2 is in the cytoplasm and ER whereas Ball is in the nucleus (Figure 4A). During the mitotic prophase, Ankle2 accumulates at the nuclear envelope but the proteins do not seem to colocalize (Figure 4B). However, at metaphase, the nuclear envelope becomes fragmented, but it does not completely dissociate in flies (Katsani et al., 2008). Ankle2 can still be seen localized to the fragmented nuclear lamina, and Ball is briefly present throughout the cytoplasm (Figure 4C). Yet, after telophase, Ball is quickly recruited back to the nucleus and briefly enriched at the nuclear envelope (Figure 4D; Video S6). After mitosis and once the chromatin is no longer condensed, Ball is nuclear. Interestingly, the spatial restriction of Ball in *Ankle2*^{A} mutants during interphase and prophase is abolished in many NBs as Ball localizes throughout the cell, a phenotype that is not observed in wild-type brains (Figures 4E and 4F, quantified in Figure S3E). In summary, Ankle2 is required for proper nuclear localization of Ball in *Drosophila*.

To determine whether ANKLE2 regulates VRK1 subcellular localization in human cells, we assayed VRK1 localization in human fibroblasts. In reference human primary fibroblasts (parental variant p.L573V/+), VRK1 is localized to the nucleus (Figure 4G) consistent with published literature indicating that VRK1 is nuclear localized (Nichols and Traktman, 2004). However, fibroblasts from microcephaly patients carrying compound heterozygous variants in *ANKLE2* (p.L573V/p.Q782* and p.V229G/p.V229G) display significantly reduced VRK1 intensity in the nucleus (Figure 4H, quantified in Figure 4I) and increased cytoplasmic staining in non-dividing cells (arrows in Figure 4H) with no significant change in overall VRK1 intensity (Figure S3F). These data argue for a conserved role between fruit flies and humans for ANKLE2 in restricting VRK1 to the nucleus.

Given that Ankle2 is required to maintain Ball-VRK1 in the nucleus during interphase, it is possible that Ball is ectopically active in the cytoplasm of *Ankle2*^{A} mutants and inhibits or promotes phosphorylation of proteins not normally encountered in the biological homeostatic state. Reducing the level of Ball may therefore alleviate the phenotype associated with the reduction in Ankle2 protein. Indeed, we observe evidence for strong dominant interactions between *Ankle2*^{A} and *ball* (multiple alleles). *Ankle2*^{A} animals are pupal lethal and have reduced brain volumes (compare Figures 4J and 4K). However, removal of one copy of *ball*, akin to a heterozygous deletion copy number variation (CNV) resulting in haploinsufficiency in humans, restores brain development (Figures 4L and 4M) and suppresses the lethality of *Ankle2*^{A} mutants (Figure 4N). Importantly, loss of one copy of *ball* (*ball*^{e107}) in *Ankle2*^{A} mutants also restores the asymmetric protein localization of aPKC and Mira crescents in metaphase NBs (Figures 4O and 4P). Hence, a partial reduction of Ball activity rescues *Ankle2*^{A} mutants, providing strong evidence for a gene dosage-sensitive locus. However, removing both copies of *ball* in wild-type animals leads to pupal lethality (Cullen et al., 2005), causes severely reduced brain volumes in 3rd instar larvae (Herzig et al., 2014), and does not rescue *Ankle2*^{A}

Figure 3. *Ankle2* Mutations Affect Asymmetric Division, Spindle Alignment, and Centrosomes

Metaphase neuroblasts stained with Baz (green, A–D), Par-6 (green, E–H), aPKC (green, I–L), and Mira (red, I–L) are shown in wild-type (A), (E), and (I); *Ankle2*^{A}/*Y* hemizygous (B), (F), and (J); *Ankle2*^{A}/*Ankle2*^{CRIMIC} transheterozygous (C), (G), and (K); and rescued (D), (H), and (L) animals. Phospho-histone H3 (pHH3; green) (A–C) and (E–K) was used to identify cell cycle stage. * notes samples where pHH3 was not used. Scale bars = 5 μm. (M–P) Quantification of phenotype severity demonstrates that *Ankle2* is required for protein localization during asymmetric division in numerous cells. Below each graph, the number of neuroblasts counted for each genotype (n) is noted. (Q–U) Metaphase neuroblasts stained with aPKC (green) and Mira (red) to mark the polarity axis and DNA (white) and Cnn (green puncta) to highlight the spindle axis from (Q) wild-type (*FRT19a*) and (R) and (S) *Ankle2* mutant neuroblasts. The angle between the spindle axis and polarity axis is measured and the percentage of metaphase neuroblasts is plotted in 15° intervals and is shown in (T) and (U). Below each group, the number of neuroblasts counted for each genotype (n) is noted.

See also Videos S2, S3, S4, and S5.

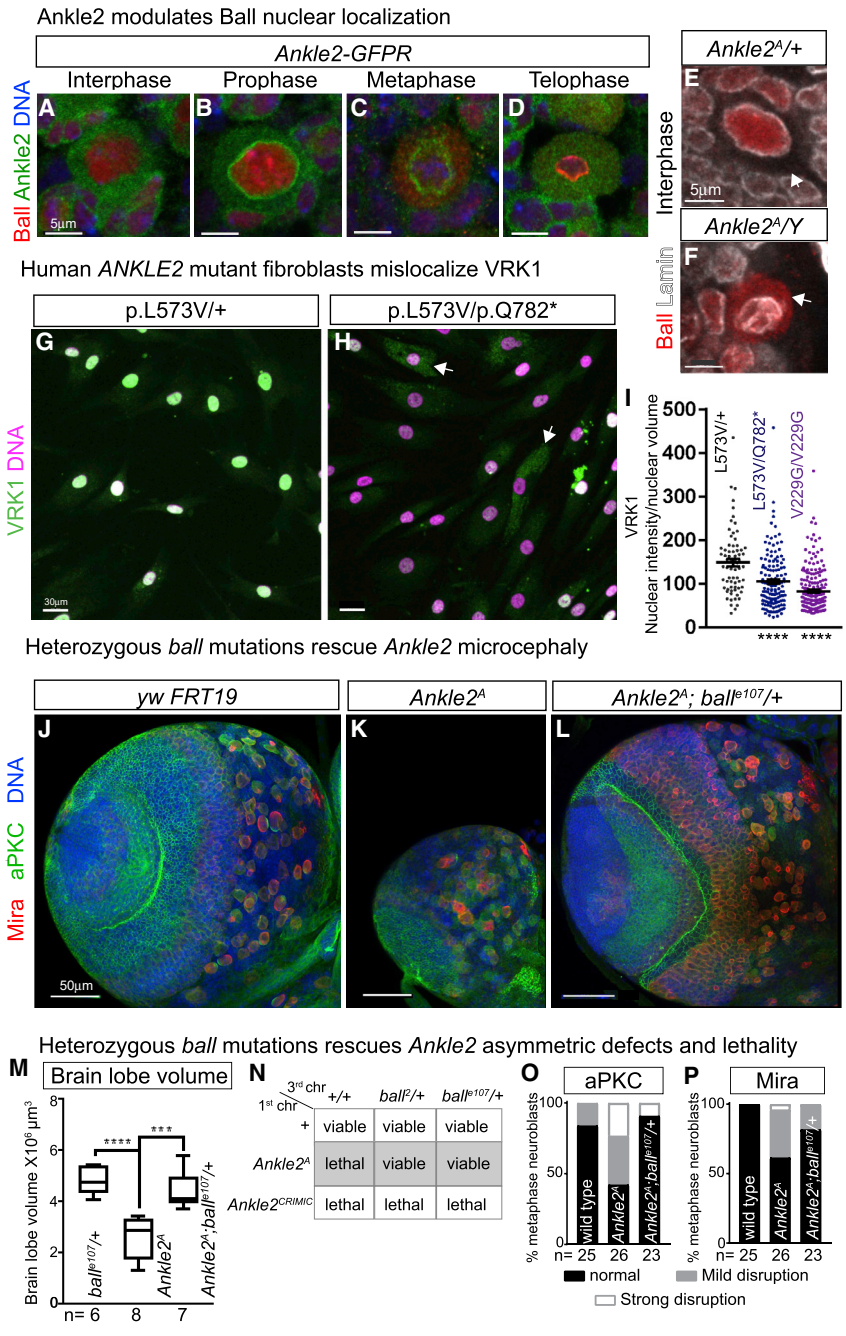

Figure 4. Ankle2 Controls Ballchen-VRK1 Localization and Function

(A–D) Immunostaining of Ankle2-GFPR (green) and Ball (red) show dynamic localizations during the cell cycle. (B) Ankle2 is localized at the nuclear envelope at prophase. Ball is nuclear (A) and (B) until nuclear envelope breakdown (C) and then localizes to the cytoplasm through the end of mitosis (D). Scale bars = 5 μm.

(E and F) Immunostaining of Ball (red) and Lamin (white) in *Ankle2^A*/+ heterozygotes and *Ankle2^A*/*Y* hemizygous mutants. Note that Lamin is disrupted and Ball becomes mislocalized throughout the cytoplasm during interphase in *Ankle2^A*/*Y* hemizygous mutants. Scale bars = 5 μm. Quantification is shown in Figure S3E.

(G and H) Confocal projections of immunostaining of VRK1 (green) and DNA (purple) in primary human fibroblasts from (G) parental unaffected (p.L573V/+) and (H) an ANKLE2 compound heterozygous patient (p.L573V/p.Q782*). VRK1 is mislocalized in fibroblasts carrying microcephaly-associated *ANKLE2* variants (p.L573V/p.Q782* and p.V229G/p.V229G), quantified as nuclear intensity in (I) as a scatter dot plot with mean and SEM plotted. Arrows in (H) indicate cytoplasmic VRK1 staining, which is minimal in (G) control fibroblasts. Scale bars = 30 μm. One-way ANOVA with multi-comparison post-test. ****p < 0.0001.

(J–L) Partial projections of 3rd instar larval brains stained with apical marker aPKC (green) and basal marker Miranda (red) in (J) wild-type (*y,w, FRT19a*), (K) *Ankle2^A*, and (L) *Ankle2^A*;;*ball^{e107}*/+ animals. Note that removal of a single copy of *ball* rescues the phenotypes of *Ankle2^A*. Scale bars = 50 μm.

(M) Quantification of 3rd instar larval brain size (as shown in (J)–(L)). n ≥ 6. One-way ANOVA with multi-comparison post-test. ****p < 0.0001, ***p < 0.001. Box plot hinges represent the 25th to 75th percentiles, a line is at the median, and whiskers represent minimum to maximum.

(N) *Ankle2^A*, but not *Ankle2^{CRIMIC}*, lethality is rescued with the introduction of multiple *ball* heterozygous mutations.

(O and P) Quantification of (O) aPKC or (P) Mira crescent intensity in 3rd instar metaphase neuroblasts in wild-type (*y w FRT19a*), *Ankle2^A* and rescued *Ankle2^A*; *ball^{e107}*/+ animals, demonstrating that *Ankle2* asymmetric division phenotypes are rescued with *ball* heterozygosity. Note that wild-type and *Ankle2^A* quantifications were shown in Figure 3. Below each graph, the number of neuroblasts or brains counted for each genotype (n) is noted.

See also Figures S3 and S5 and Video S6.

animals, emphasizing that the gene dosage and balance of the protein levels is critical. Indeed, a severe loss-of-function allele, *Ankle2^{CRIMIC}*, cannot be suppressed by reducing Ball activity (Figure 4N). In summary, these data demonstrate that both Ankle2 and Ball-VRK1 control the distribution of asymmetric determinants, and experimental evidence reveals an antagonistic relationship between both proteins.

The Ankle2-Ball Pathway Modulates aPKC and L(2)gl

Because of the similarities in defects observed with the loss of *Ankle2* or *aPKC*, including mislocalization of Par-6 and Mira (Kim et al., 2009), decreased cell divisions, and reduced NB clone volume (Rolls et al., 2003), we hypothesized that the activity of aPKC, an important mediator of NB asymmetric division (Figure 5A), might be affected. aPKC phosphorylation (Kim et al., 2009) or abundance could be modulated by Ankle2. We therefore assessed both total and phosphorylated aPKC (p-aPKC) levels in third instar larval brains using an antibody specific for human p-aPKC T410 (T422 in flies). This phosphorylation site is located in its activation loop and was shown to be important for its kinase activity (Kim et al., 2009). Phosphorylation of aPKC (T422) relative to total aPKC is decreased in *Ankle2*

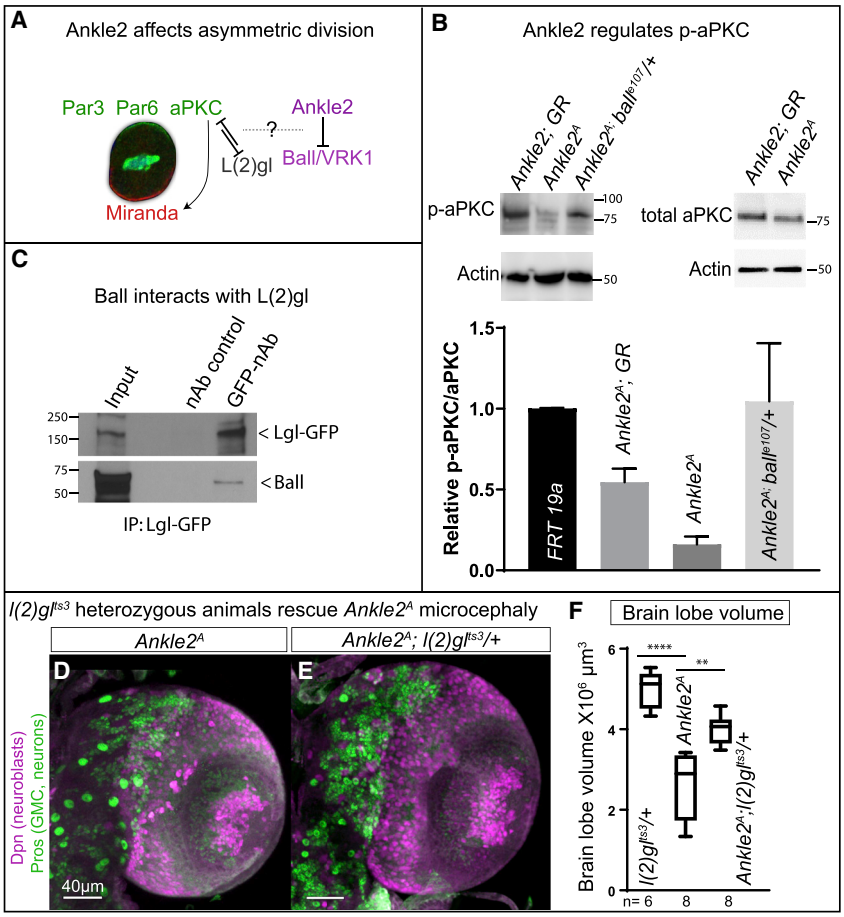

Figure 5. Ankle2 Affects Asymmetric Division through aPKC and L(2)gl

(A) Ankle2 and Ball regulate asymmetric division.

(B) Western analysis of phosphorylated aPKC in larval brains (mammalian T410 corresponds to T422 in *Drosophila*) from genomic rescue (GR) (*Ankle2^{A}; Ankle2-GFPR*), *Ankle2^{A}*, and *Ankle2^{A};; ball^{e107}/+* animals or total aPKC levels in GR (*Ankle2^{A}; Ankle2-GFPR*) and *Ankle2^{A}* mutants. Note that p-aPKC is reduced in *Ankle2* mutants but restored with the introduction of GR or reduction of Ball and is quantified as the ratio of p-aPKC to total aPKC. n = 3 replicates. Bar graph represents mean and error bars represent standard deviation.

(C) *In vivo* immunoprecipitation of L(2)gl-GFP using GFP-nAb in *L(2)gl$^{MI07575\text{-}GFSTF}$* larvae demonstrates L(2)gl can interact with Ball *in vivo*.

(D and E) Partial projections of third instar larval brains stained for Dpn (purple, neuroblasts) and Pros (green, daughter cells and neurons) of (D) *Ankle2^{A}* and (E) *Ankle2^{A}/+;l(2)gl^{ts3}* mutant animals raised at 22°C with brain volume quantified in (F). Scale bars = 40 µm. Note that reduction of L(2)gl in an *Ankle2^{A}* hemizygous animal rescues brain size defects and lethality at 22°C. Box plot hinges represent the 25th to 75th percentiles, a line is at the median, and whiskers represent minimum to maximum. One-way ANOVA with multi-comparison post-test. **p < 0.01, ****p < 0.0001. Below the graph, the number of brains counted for each genotype (n) is noted.

See also Figure S6.

mutants (Figure 5B) and is restored with either addition of Ankle2-GFPR or reduction of *ball* (Figure 5B), consistent with the data presented in Figure 4. However, overexpression of aPKC or constitutively active aPKC (aPKC$^{\Delta N}$) (Betschinger et al., 2003) in *Ankle2^{A}* mutants did not rescue brain size or viability (data not shown).

aPKC has been shown to physically interact with L(2)gl (Betschinger et al., 2003), a regulator of apico-basal polarity that inhibits the function of aPKC (Atwood and Prehoda, 2009; Wirtz-Peitz et al., 2008). *aPKC* and *l(2)gl* genetically interact as removal of one copy of *aPKC* suppresses *l(2)gl* loss-of-function phenotypes (Rolls et al., 2003), and aPKC has been shown to phosphorylate L(2)gl to control its plasma membrane or cortical release (Betschinger et al., 2003). When aPKC is active, L(2)gl is phosphorylated and released from the cortex; once released, it no longer binds to aPKC or inhibits its function. Because aPKC and L(2)gl interact, the Ankle2-Ball pathway may affect L(2)gl. We therefore assessed whether L(2)gl physically interacts with the Ankle2-Ball pathway using immunoprecipitation of a GFP-tagged L(2)gl from third instar larval brains and found that Ball indeed interacts with L(2)gl (Figure 5C).

The reduced aPKC activity that we observe may be associated with a gain of function of L(2)gl. Therefore, to determine whether removal of one copy of *l(2)gl* suppresses *Ankle2*-associated phenotypes, we introduced a temperature-sensitive mutation of *l(2)gl (l(2)gl^{ts3})* into the *Ankle2^{A}* mutant background and found that reducing *l(2)gl* in *Ankle2^{A}* mutants at 22°C (Figures 5D–5F) and 25°C indeed partially restored brain size. *Ankle2^{A}* is pupal lethal at 22°C, but when combined with a heterozygous *l(2)gl* mutant allele, some *Ankle2^{A}* animals survive to adulthood. However, unlike the removal of one copy of *ball*, these animals die a few days after eclosion. In summary, Ankle2 and Ball interact with the apical-basal polarity regulators aPKC and L(2)gl (Figure 5A) and affect aPKC and L(2)gl activity by disturbing the asymmetric segregation of apical-basal polarity factors in NBs. Our data suggest that in *Ankle2* mutants, L(2)gl acts as a gain of function (increased activity), and aPKC activity is reduced. Therefore, by reducing L(2)gl activity, aPKC function is restored.

Disease -Associated Variants in *VRK1* and Its Paralogs

Ten families have been described with biallelic variants in *VRK1* that cause a spectrum of neurologic diseases including 6 individuals with microcephaly (Feng et al., 2019; Gonzaga-Jauregui et al., 2013; Najmabadi et al., 2011; Nguyen et al., 2015; Renbaum et al., 2009; Shaheen et al., 2019; Stoll et al., 2016) (Table S1; Figure S5). The family structures suggest either a sporadic or recessive neurological disease trait; historical consanguinity in 3 of 10 pedigrees implicate an autosomal recessive locus. Screening the BHCMG and BG databases identified two additional families with potentially biallelic variants in *VRK1*. (Table S2; Figure S5). These cases suggest that similar to *ANKLE2* (Figure S1), a heterogenous set of variant alleles in *VRK1* are associated with neurologic disease and microcephaly.

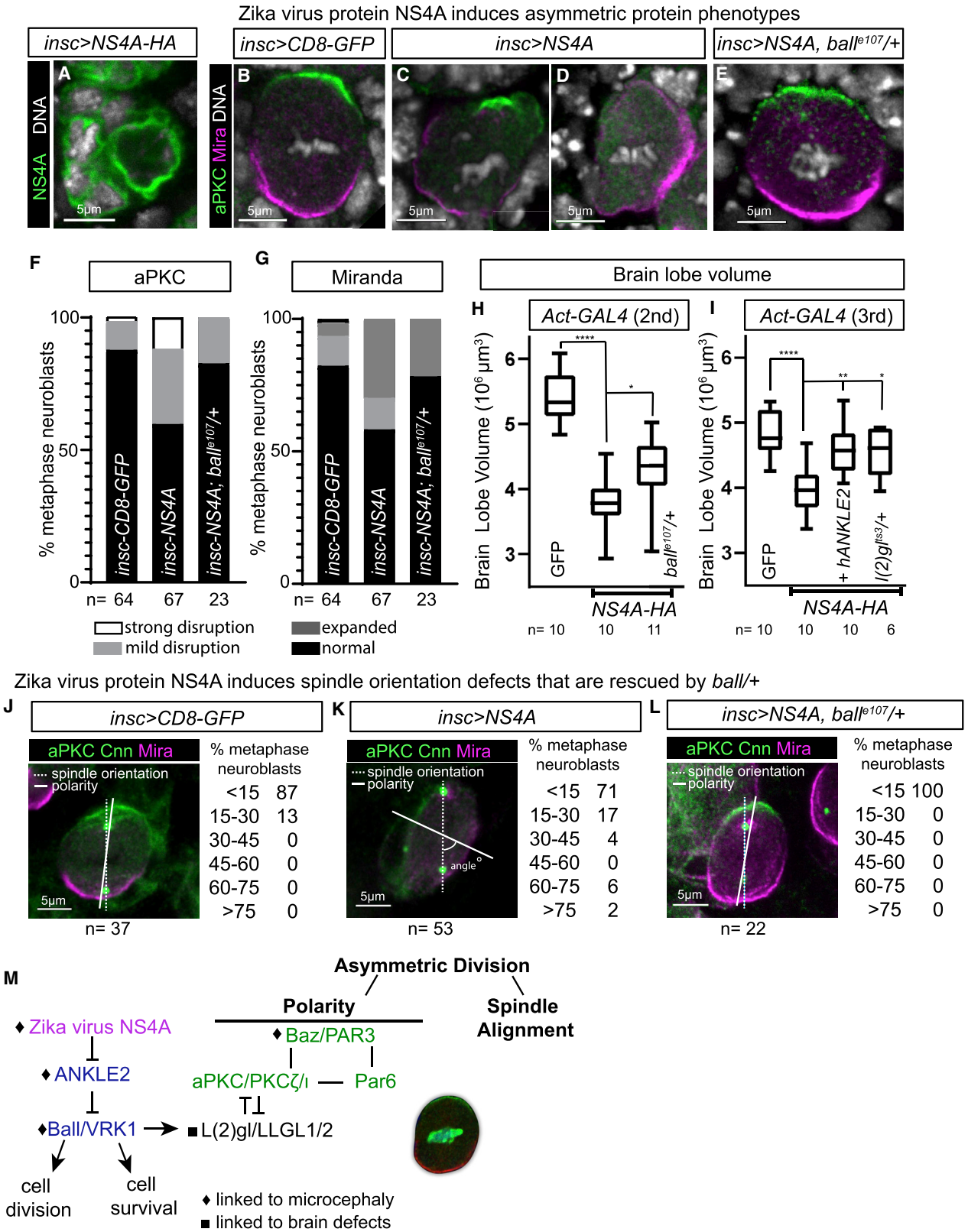

Figure 6. Zika Virus NS4A Targets the Ankle2 Pathway

(A) 3rd instar brains with neuroblast-specific (*insc-GAL4*) NS4A-HA expression stained for HA (green) and DNA (white) show that NS4A localizes in a pattern similar to Ankle2 (Figure 2). Scale bar = 5 µm.

(legend continued on next page)

It was previously shown that fly genes with more than one human homolog, especially those that are evolutionarily conserved, have an enriched association with Online Mendelian Inheritance in Man (OMIM) disease phenotypes (Yamamoto et al., 2014), which is a comprehensive and authoritative catalog of human genes and genetic phenotypes associated with mendelian disorders. We searched the BHCMG database to establish if damaging variants in paralogs of *VRK1* are associated with disease. Predicted deleterious, biallelic variants were found in two paralogs of *VRK1*: *VRK2* is associated with very small eyes and *VRK3* with severe microcephaly (Table S2; Figure S6).

NS4A Targets the Ankle2 Pathway

Drosophila has been developed as a model of viral infection (Harsh et al., 2018; Liu et al., 2018), and we recently showed that expression of the Zika virus protein NS4A results in reduced brain size in *Drosophila* (Shah et al., 2018). Strikingly, NS4A expression in $Ankle2^{A}$/+ heterozygous animals leads to a more severe phenotype than NS4A expression in a wild-type background, and these animals display brain phenotypes that mimic $Ankle2^{CRIMIC}$ null mutants (Shah et al., 2018). These data again suggest that levels of Ankle2 protein are critical. In our previous experiments, we were unable to detect NS4A using immunohistochemistry. We therefore generated an additional NS4A construct with a C-terminal HA tag (*UAS-NS4A-HA*) and drove expression with *insc-GAL4>UAS-NS4A-HA*. As shown in Figure 6A, NS4A is localized to the nuclear envelope and ER (Figure 6A), similar to the subcellular localization of Ankle2 (Figure 2). Expression of NS4A may cause brain defects by affecting aPKC and Mira localization. Indeed, expression of NS4A in NBs (*insc-GAL4>UAS-NS4A*) affects the apical aPKC localization and leads to an expansion of the Mira domain (Figure 6B compared to Figures 6C and 6D and quantified in Figures 6F and 6G). In the metaphase NBs that express NS4A, we also note spindle orientation defects in some cells (Figures 6J and 6K), similar to $Ankle2^{A}$ animals shown in Figure 3. These data indicate that NS4A targets the Ankle2 pathway; this is further strengthened with the observation that when NS4A is expressed in NBs of *ball* heterozygous animals, aPKC and Mira crescents are restored to their wild-type patterns (Figures 6E–6G), and spindle orientation defects are rescued (compare Figure 6L with Figure 6K). Finally, ubiquitous expression of NS4A-HA (Figures 6H and 6I) using two different *Act-GAL4* insertions causes reduced brain volume (Figure 6H) that is rescued by removal of one copy of *ball*, (Figure 6I) co-expression of human ANKLE2, or (Figure 6I) removal of one copy of *l(2)gl*. In summary, the Zika virus protein NS4A targets the Ankle2 pathway and affects asymmetric distribution of cell fate determinants, leading to defects in NB division and brain development.

DISCUSSION

We investigated the biological basis for *ANKLE2*-associated microcephaly. We report six additional patients with microcephaly that carry mutations in *ANKLE2* and show that three variants identified in probands cause a loss of *ANKLE2* function when tested in flies (Figures 1 and S1), providing compelling evidence that its loss causes reduced brain size in flies and severe microcephaly (Z score < -2.5) in humans. *Ankle2* is a dosage-sensitive locus whose product is inhibited by the Zika virus protein NS4A. We show that Ankle2, similar to NS4A, is localized to the ER and that it targets the nuclear envelope during mitosis. Loss of *Ankle2* affects the nuclear envelope and ER distribution and results in a redistribution of Ball or VRK1, a kinase that is normally localized to the nucleus except when the nuclear envelope breaks down during mitosis (Figure 4). Loss of *Ankle2* disrupts the localization of NB apical-basal polarity determinants such as aPKC, Par-6, Baz, and Mir, and aPKC phosphorylation is reduced by *Ankle2* mutations. Importantly, loss of one copy of *ball* or *l(2)gl* suppresses the reduced brain volume associated with a partial loss of *Ankle2*, suggesting that much of the biological function of Ankle2 is modulated by aPKC and L(2)gl. Finally, the negative influence of NS4A on the activity of ANKLE2 can also be suppressed by removal of one copy of *ball* or *l(2)gl*, suggesting the following pathway: NS4A ⊣ ANKLE2 ⊣ Ball-VRK1 → L(2)gl-LLGL1 ⊣ aPKC. This pathway, regulated by ANKLE2, plays an important role in NB stem cell divisions in flies and microcephaly and potentially other neurological disease phenotypes in humans.

Interestingly, the above pathway links environmental cues with several genetic causes of sporadic and autosomal recessive microcephaly in humans; moreover, it implicates this pathway in microcephaly accompanying congenital infection. As one example of the latter, the Zika virus has been shown to cross the infant blood brain barrier (Mlakar et al., 2016) and has been identified in radial glial cells (Li et al., 2016) as well as intermediate progenitor cells and neurons (Lin et al., 2017). We propose that NS4A affects the function of Ankle2 leading to the release of Ball-VRK1 from the nucleus. We speculate that this in turn

(B–G) Metaphase neuroblasts stained for aPKC (green) and Mira (purple) in brains with neuroblast-specific (*insc-GAL4*) expression of (B) *CD8-GFP*, (C) and (D) *NS4A*, or (E) *NS4A* in $ball^{e107}$ heterozygous animals. Scale bars = 5 μm. aPKC and Mira crescent intensities are quantified in (F) and (G).

(H) Brain volume quantification from animals with ubiquitous expression of *CD8-GFP* (control), *NS4A-HA*, or *NS4A-HA* in $ball^{e107}$ heterozygous animals using *Act-GAL4* on the 2nd chromosome. ****$p < 0.0001$, *$p < 0.05$. Box plot hinges represent the 25th to 75th percentiles, a line is at the median, and whiskers represent minimum to maximum.

(I) *Act-GAL4* (3rd chromosome) ubiquitous expression of *CD8-GFP* (control), *NS4A-HA*, *NS4A-HA* and human *ANKLE2*, or *NS4A-HA* in $l(2)gl^{ts3}$ heterozygous animals. Note that human ANKLE2 expression or reduction of Ball or L(2)gl activity rescues NS4A induced brain defects. One-way ANOVA with multi-comparison post-test. ****$p < 0.0001$, **$p < 0.01$, *$p < 0.05$. Box plot hinges represent the 25th to 75th percentiles, a line is at the median, and whiskers represent minimum to maximum.

(J–L) aPKC (green), Cnn (green), and Mira (purple) staining of metaphase neuroblasts with *insc-GAL4* expression of (J) *CD8-GFP*, (K) *NS4A*, and (M) *NS4A* in $ball^{e107}$ heterozygous animals. The angle between the spindle axis and polarity axis is measured and percent of total metaphase neuroblasts is noted at 15° intervals. Expression of NS4A causes localization defects of aPKC and Mira and spindle orientation defects in metaphase neuroblasts.

(M) Zika virus NS4A inhibits the ANKLE2-VRK1 pathway, which regulates asymmetric determinant localization as well as the division axes.

affects the phosphorylation of aPKC and L(2)gl directly by masking phosphorylation sites or indirectly by promoting the activity of one or more phosphatases. Loss of VRK1 has been shown to cause microcephaly and some variant alleles are also associated with pontocerebellar hypoplasia (PCH) in humans (Gonzaga-Jauregui et al., 2013; Renbaum et al., 2009), consistent with the loss of *ball* in flies that causes a severe reduction in brain size (Yakulov et al., 2014). Note that ANKLE2, VRK1, LLGL1, and aPKC as well as other components of the apical complex such as PARD3 are all present in radial glial cells during cortical development (Ayoub et al., 2011). These data suggest that ANKLE2 and its partners such as LLGL1 and asymmetric determinants are important proteins during neural cell proliferation and that the proper levels and relative amounts of these proteins determine how many neurons will eventually be formed in vertebrates. Our data also indicate that variant alleles at either *ANKLE2* or *VRK1* are responsible for some causes of embryonic lethality and severe congenital microcephaly.

LLGL1 has recently been shown to play an important role in radial glia in mice during neurogenesis, and its loss in clones increases the number of divisions (Beattie et al., 2017). In addition, aPKCζ or λ localizes at the apical membrane of proliferating neural stem cells in chicken embryos during division and has been shown to provide an instructive signal for apical assembly of adherens junctions (Ghosh et al., 2008). Mouse knockouts of *aPKCλ* (Soloff et al., 2004) and *aPKCι* (Seidl et al., 2013) are embryonic lethal; however, *aPKCζ* knockouts are viable (Leitges et al., 2001), perhaps suggesting redundant functions within the aPKC family. These proteins have not been linked to microcephaly in mice, but conditional removal of an apical complex protein Pals1 in cortical progenitors resulted in complete cortex loss (Kim et al., 2010). Finally, Numb is asymmetrically localized by the Par complex protein in *Drosophila*, segregated to the daughter cell during asymmetric cell division (Wirtz-Peitz et al., 2008), and essential for daughter cells to adopt distinct fates (Bhalerao et al., 2005). In mice, Numb localization is also asymmetric and null mutations exhibit embryonic lethality, neural tube closure defects, and premature neuron development (Zhong et al., 2000). These data indicate that asymmetric division may be important for vertebrate neuronal development, but microcephaly is not a phenotype that typically associates with loss of the mice homologs of asymmetric-localized determinants identified in *Drosophila*. However, the observations reported here indicate that the ANKLE2-PAR complex pathway is evolutionarily conserved from flies to humans, although the precise mechanisms remain to be determined as different cells may use this pathway in different contexts (Suzuki and Ohno, 2006).

In order to determine whether predicted deleterious biallelic variants in PAR-complex-encoding genes or their paralogs associated with a neurologic disease trait, we searched the BHCMG database for mutations associated with neurological disease. We found homozygous predicted deleterious missense variants in *PARD3B* (c.1222G>A, p.G408S) in a patient that has microcephaly (Table S2; Figure S6) and compound heterozygous mutations in *PARD3B* (c.1654G>A, p.A552T) that are associated with other neurological defects (Table S2; Figure S6). The human ortholog of *L(2)gl*, *LLGL1*, is deleted in Smith-Magenis syndrome (SMS) (Smith et al., 1986), and 86%–89% of the SMS patients have brachycephaly (Greenberg et al., 1996). These observations extend the mutational load beyond *ANKLE2* and *VRK1* and suggest an association between congenital disease and variants within the PAR complex (Table S2; Figure S6), potentially by a compound inheritance gene dosage model (Wu et al., 2015).

The Aurora A (AurA) kinase has been shown to phosphorylate the Par complex (Wirtz-Peitz et al., 2008) as well as L(2)gl (Carvalho et al., 2015) and regulates cortical polarity and spindle orientation in NBs (Lee et al., 2006; Wang et al., 2006). The aberrant localization of Ball-VRK1 in *Ankle2* mutants may lead to gain-of-function phenotypes that are highly dosage sensitive, as they can be repressed by removing a single copy of Ball-VRK1 in $Ankle2^{A}$. Mislocalized Ball-VRK1 may mask or interfere with the function of AurA in NB asymmetric division as they share similar kinase substrate consensus sequences (Sanz-García et al., 2011; Ferrari et al., 2005). Future studies are needed to assess Ball-VRK1 redundancy or interference with AurA function.

Another possible evolutionarily parallel with implications in multicellular organismal development is the genetic interaction between the *C. elegans* homolog of VRK1 and an ANKLE2-like protein at the two-cell stage (Asencio et al., 2012). Whereas VRK1 in both *Drosophila* and humans (Nichols and Traktman, 2004) is localized to the nucleus, except during mitosis when the nuclear envelope is broken down (Figure 4), the worm VRK1 protein is localized to the nuclear envelope. The worm ANKLE2-like protein, Lem-4L, also interacts with the phosphatase PP2A (Asencio et al., 2012), and the fly PP2A regulates NB asymmetric division by interacting with aPKC and excluding it from the basal cortex (Chabu and Doe, 2009; Ogawa et al., 2009; Wang et al., 2009). PP2A also antagonizes the phosphorylation of Baz by PAR-1 to control apical-basal polarity in dividing embryonic NBs (Krahn et al., 2009) and regulates Baz localization in other cells such as neurons (Nam et al., 2007). This raises the possibility that the Ankle2 pathway also acts with PP2A in NB asymmetric division.

Here, we identified a pathway that plays a significant role in NB asymmetric division. By combining functional studies in *Drosophila* together with human subject data, we have linked several microcephaly-associated genes and congenital infection to a single genetic pathway. These studies allowed us to highlight conserved functions of the ANKLE2 pathway and provide mechanistic insight into how a Zika infection might affect asymmetric division. This *ANKLE2-VRK1* gene dosage-sensitive pathway can be perturbed by genetic variants that disturb biological homeostasis resulting in neurological disease traits or by environmental insults such as Zika virus impinging on neurodevelopment. Hence, lessons learned from the study of rare diseases can provide insights into more common diseases and potential gene- environment interactions.

STAR★METHODS

Detailed methods are provided in the online version of this paper and include the following:

- KEY RESOURCES TABLE
- LEAD CONTACT AND MATERIALS AVAILABILITY
- EXPERIMENTAL MODEL AND SUBJECT DETAILS
  - Drosophila melanogaster
  - Human Studies

SUPPLEMENTAL INFORMATION

Supplemental Information can be found online at https://doi.org/10.1016/j.devcel.2019.10.009.

ACKNOWLEDGMENTS

We would like to thank many members of the Bellen lab for suggestions and Megan Campbell and Karen Schulze for critical reading. We thank Chris Doe, Jurgen Knoblich, Jim Skeath, Kenneth Prehoda, Alf Herzig, Hiroyuki Ohkura, and the Bloomington *Drosophila* Stock Center for providing stocks and reagents and the IDDRC Microscopy Core (NIH/NICHD U54 HD083092) for valuable input. This work was supported by NIH/NINDS F32NS092270 to N.L.; Howard Hughes Medical Institute (HHMI) Medical Research Fellowship to A.J.; the NIH/NINDS K08NS092898 and Jordan's Guardian Angels to G.M.M.; a jointly funded NHGRI and NHLBI grant to the Baylor-Hopkins Center for Mendelian Genomics (UM1 HG006542); NIH/NINDS R35NS105078 to J.R.L; and NIH U54NS093793, NIH R24OD022005, and the Huffington Foundation to H.J.B. N.L. and H.C. are supported by HHMI and H.J.B. is an Investigator of the Howard Hughes Medical Institute.

AUTHOR CONTRIBUTIONS

N.L. and H.J.B. conceived the project, designed the experiments, and wrote and revised the manuscript with J.R.L. H.C. performed the *in vivo* Ankle2 immunoprecipitations and assessed protein levels. A.J. assisted with the brain volume measurements. A.J., M.W., and J.R.L. performed the primary fibroblast experiments and human mutation studies. H.A., B.B.G., T.T., S.I., B.T., G.M.M., G.H.M., A.X.T., and R.D.C. ascertained the clinical and molecular data of children with variants. B.T., B.R.A., P.S.S., and N.J.K. assisted with the Zika virus experiments. N.L. performed all other experiments.

DECLARATION OF INTERESTS

The authors declare no competing interests.

Received: May 13, 2019
Revised: August 19, 2019
Accepted: October 14, 2019
Published: November 14, 2019

REFERENCES

Andersen, R.O., Turnbull, D.W., Johnson, E.A., and Doe, C.Q. (2012). Sgt1 acts via an LKB1/AMPK pathway to establish cortical polarity in larval neuroblasts. Dev. Biol. *363*, 258–265.

Asencio, C., Davidson, I.F., Santarella-Mellwig, R., Ly-Hartig, T.B., Mall, M., Wallenfang, M.R., Mattaj, I.W., and Gorjánácz, M. (2012). Coordination of kinase and phosphatase activities by Lem4 enables nuclear envelope reassembly during mitosis. Cell *150*, 122–135.

Atwood, S.X., Chabu, C., Penkert, R.R., Doe, C.Q., and Prehoda, K.E. (2007). Cdc42 acts downstream of Bazooka to regulate neuroblast polarity through Par-6 aPKC. J. Cell Sci. *120*, 3200–3206.

Atwood, S.X., and Prehoda, K.E. (2009). aPKC phosphorylates Miranda to polarize fate determinants during neuroblast asymmetric cell division. Curr. Biol. *19*, 723–729.

Ayoub, A.E., Oh, S., Xie, Y., Leng, J., Cotney, J., Dominguez, M.H., Noonan, J.P., and Rakic, P. (2011). Transcriptional programs in transient embryonic zones of the cerebral cortex defined by high-resolution mRNA sequencing. Proc. Natl. Acad. Sci. U S A *108*, 14950–14955.

Bamshad, M.J., Shendure, J.A., Valle, D., Hamosh, A., Lupski, J.R., Gibbs, R.A., Boerwinkle, E., Lifton, R.P., Gerstein, M., Gunel, M., et al. (2012). The Centers for Mendelian Genomics: a new large-scale initiative to identify the genes underlying rare Mendelian conditions. Am. J. Med. Genet. A *158A*, 1523–1525.

Barton, L.J., Soshnev, A.A., and Geyer, P.K. (2015). Networking in the nucleus: a spotlight on LEM-domain proteins. Curr. Opin. Cell Biol. *34*, 1–8.

Beattie, R., Pia Postiglione, M., Burnett, L., Laukoter, S., Streicher, C., Pauler, F., Xiao, G., Klezovitch, O., Vasioukhin, V., Ghashghaei, T., and Hippenmeyer, S. (2017). Mosaic analysis with double markers reveals distinct sequential functions of Lgl1 in neural stem cells. Neuron *94*, 517–533.

Betschinger, J., Mechtler, K., and Knoblich, J.A. (2003). The Par complex directs asymmetric cell division by phosphorylating the cytoskeletal protein Lgl. Nature *422*, 326–330.

Bhalerao, S., Berdnik, D., Török, T., and Knoblich, J.A. (2005). Localization-dependent and -independent roles of numb contribute to cell-fate specification in Drosophila. Curr. Biol. *15*, 1583–1590.

Bier, E., Vaessin, H., Younger-Shepherd, S., Jan, L.Y., and Jan, Y.N. (1992). deadpan, an essential pan-neural gene in Drosophila, encodes a helix-loop-helix protein similar to the hairy gene product. Genes Dev. *6*, 2137–2151.

Bischof, J., Björklund, M., Furger, E., Schertel, C., Taipale, J., and Basler, K. (2013). A versatile platform for creating a comprehensive UAS-ORFeome library in Drosophila. Development *140*, 2434–2442.

Bonaccorsi, S., Mottier, V., Giansanti, M.G., Bolkan, B.J., Williams, B., Goldberg, M.L., and Gatti, M. (2007). The Drosophila LKB1 kinase is required for spindle formation and asymmetric neuroblast division. Development *134*, 2183–2193.

Brunetti-Pierri, N., Berg, J.S., Scaglia, F., Belmont, J., Bacino, C.A., Sahoo, T., Lalani, S.R., Graham, B., Lee, B., Shinawi, M., et al. (2008). Recurrent reciprocal 1q21.1 deletions and duplications associated with microcephaly or macrocephaly and developmental and behavioral abnormalities. Nat. Genet. *40*, 1466–1471.

Cabernard, C., and Doe, C.Q. (2009). Apical/basal spindle orientation is required for neuroblast homeostasis and neuronal differentiation in Drosophila. Dev. Cell *17*, 134–141.

Campbell, G., Göring, H., Lin, T., Spana, E., Andersson, S., Doe, C.Q., and Tomlinson, A. (1994). RK2, a glial-specific homeodomain protein required for embryonic nerve cord condensation and viability in Drosophila. Development *120*, 2957–2966.

Carvalho, C.A., Moreira, S., Ventura, G., Sunkel, C.E., and Morais-de-Sá, E. (2015). Aurora A triggers Lgl cortical release during symmetric division to control planar spindle orientation. Curr. Biol. *25*, 53–60.

Chabu, C., and Doe, C.Q. (2008). Dap160/intersectin binds and activates aPKC to regulate cell polarity and cell cycle progression. Development *135*, 2739–2746.

Chabu, C., and Doe, C.Q. (2009). Twins/PP2A regulates aPKC to control neuroblast cell polarity and self-renewal. Dev. Biol. *330*, 399–405.

Clarkson, M., and Saint, R. (1999). A His2AvDGFP fusion gene complements a lethal His2AvD mutant allele and provides an in vivo marker for Drosophila chromosome behavior. DNA Cell Biol. *18*, 457–462.

Cullen, C.F., Brittle, A.L., Ito, T., and Ohkura, H. (2005). The conserved kinase NHK-1 is essential for mitotic progression and unifying acentrosomal meiotic spindles in Drosophila melanogaster. J. Cell Biol. *171*, 593–602.

Devhare, P., Meyer, K., Steele, R., Ray, R.B., and Ray, R. (2017). Zika virus infection dysregulates human neural stem cell growth and inhibits differentiation into neuroprogenitor cells. Cell Death Dis. *8*, e3106.

Drier, E.A., Tello, M.K., Cowan, M., Wu, P., Blace, N., Sacktor, T.C., and Yin, J.C. (2002). Memory enhancement and formation by atypical PKM activity in Drosophila melanogaster. Nat. Neurosci. *5*, 316–324.

Dumas, L.J., O'Bleness, M.S., Davis, J.M., Dickens, C.M., Anderson, N., Keeney, J.G., Jackson, J., Sikela, M., Raznahan, A., Giedd, J., et al. (2012). DUF1220-domain copy number implicated in human brain-size pathology and evolution. Am. J. Hum. Genet. *91*, 444–454.

Feng, S.Y., Li, L.Y., Feng, S.M., and Zou, Z.Y. (2019). A novel VRK1 mutation associated with recessive distal hereditary motor neuropathy. Ann. Clin. Transl. Neurol. *6*, 401–405.

Ferrari, S., Marin, O., Pagano, M.A., Meggio, F., Hess, D., El-Shemerly, M., Krystyniak, A., and Pinna, L.A. (2005). Aurora-A site specificity: a study with synthetic peptide substrates. Biochem. J. *390*, 293–302.

Gallaud, E., Pham, T., and Cabernard, C. (2017). Drosophila melanogaster neuroblasts: a model for asymmetric stem cell divisions. Results Probl. Cell Differ. *61*, 183–210.

Gateff, E., and Schneiderman, H.A. (1974). Developmental capacities of benign and malignant neoplasms of Drosophila. Wilhelm Roux Arch. Entwickl. Mech. Org. *176*, 23–65.

Ghosh, S., Marquardt, T., Thaler, J.P., Carter, N., Andrews, S.E., Pfaff, S.L., and Hunter, T. (2008). Instructive role of aPKCzeta subcellular localization in the assembly of adherens junctions in neural progenitors. Proc. Natl. Acad. Sci. U S A *105*, 335–340.

Gonzaga-Jauregui, C., Lotze, T., Jamal, L., Penney, S., Campbell, I.M., Pehlivan, D., Hunter, J.V., Woodbury, S.L., Raymond, G., Adesina, A.M., et al. (2013). Mutations in VRK1 associated with complex motor and sensory axonal neuropathy plus microcephaly. JAMA Neurol. *70*, 1491–1498.

Gonzaga-Jauregui, C., Lupski, J., and Gibbs, R. (2012). Human genome sequencing in health and disease. Annu. Rev. Med. *63*, 35–61.

Greenberg, F., Lewis, R.A., Potocki, L., Glaze, D., Parke, J., Killian, J., Murphy, M.A., Williamson, D., Brown, F., Dutton, R., et al. (1996). Multi-disciplinary clinical study of Smith-Magenis syndrome (deletion 17p11.2). Am. J. Med. Genet. *62*, 247–254.

Harsh, S., Ozakman, Y., Kitchen, S.M., Paquin-Proulx, D., Nixon, D.F., and Eleftherianos, I. (2018). Dicer-2 regulates resistance and maintains homeostasis against Zika virus infection in Drosophila. J. Immunol. *201*, 3058–3072.

Herzig, B., Yakulov, T.A., Klinge, K., Günesdogan, U., Jäckle, H., and Herzig, A. (2014). Bällchen is required for self-renewal of germline stem cells in Drosophila melanogaster. Biol. Open *3*, 510–521.

Homem, C.C., and Knoblich, J.A. (2012). Drosophila neuroblasts: a model for stem cell biology. Development *139*, 4297–4310.

Ito, K., Awano, W., Suzuki, K., Hiromi, Y., and Yamamoto, D. (1997). The Drosophila mushroom body is a quadruple structure of clonal units each of which contains a virtually identical set of neurones and glial cells. Development *124*, 761–771.

Jayaraman, D., Bae, B.I., and Walsh, C.A. (2018). The genetics of primary microcephaly. Annu. Rev. Genomics Hum. Genet. *19*, 177–200.

Kanai, M.I., Kim, M.J., Akiyama, T., Takemura, M., Wharton, K., O'Connor, M.B., and Nakato, H. (2018). Regulation of neuroblast proliferation by surface glia in the Drosophila larval brain. Sci. Rep. *8*, 3730.

Karaca, E., Posey, J.E., Coban Akdemir, Z., Pehlivan, D., Harel, T., Jhangiani, S.N., Bayram, Y., Song, X., Bahrambeigi, V., Yuregir, O.O., et al. (2018). Phenotypic expansion illuminates multilocus pathogenic variation. Genet. Med. *20*, 1528–1537.

Katsani, K.R., Karess, R.E., Dostatni, N., and Doye, V. (2008). In vivo dynamics of Drosophila nuclear envelope components. Mol. Biol. Cell *19*, 3652–3666.

Kim, S., Gailite, I., Moussian, B., Luschnig, S., Goette, M., Fricke, K., Honemann-Capito, M., Grubmüller, H., and Wodarz, A. (2009). Kinase-activity-independent functions of atypical protein kinase C in Drosophila. J. Cell Sci. *122*, 3759–3771.

Kim, S., Lehtinen, M., Sess, A., Zappaterra, M., Cho, S.-H., Gonzalez, D., Boggan, B., Austin, C., Wijnholds, J., Gambello, M., Malicki, J., LaMantia, A., Broccoli, V., and Walsh, C. (2010). The apical complex couples cell fate and cell survival to cerebral cortical development. Neuron *66*, 69–84.

Kondo, S., and Ueda, R. (2013). Highly improved gene targeting by germline-specific Cas9 expression in Drosophila. Genetics *195*, 715–721.

Krahn, M.P., Egger-Adam, D., and Wodarz, A. (2009). PP2A antagonizes phosphorylation of Bazooka by PAR-1 to control apical-basal polarity in dividing embryonic neuroblasts. Dev. Cell *16*, 901–908.

Lee, C.Y., Andersen, R.O., Cabernard, C., Manning, L., Tran, K.D., Lanskey, M.J., Bashirullah, A., and Doe, C.Q. (2006). Drosophila aurora-A kinase inhibits neuroblast self-renewal by regulating aPKC/Numb cortical polarity and spindle orientation. Genes Dev. *20*, 3464–3474.

Lee, P.T., Zirin, J., Kanca, O., Lin, W.W., Schulze, K.L., Li-Kroeger, D., Tao, R., Devereaux, C., Hu, Y., Chung, V., et al. (2018). A gene-specific *T2A-GAL4* library for *Drosophila*. ELife *7*, e35574.

Lee, T., and Luo, L. (2001). Mosaic analysis with a repressible cell marker (MARCM) for Drosophila neural development. Trends Neurosci. *24*, 251–254.

Leitges, M., Sanz, L., Martin, P., Duran, A., Braun, U., García, J.F., Camacho, F., Diaz-Meco, M.T., Rennert, P.D., and Moscat, J. (2001). Targeted disruption of the zetaPKC gene results in the impairment of the NF-kappaB pathway. Mol. Cell *8*, 771–780.

Li, C., Xu, D., Ye, Q., Hong, S., Jiang, Y., Liu, X., Zhang, N., Shi, L., Qin, C.F., and Xu, Z. (2016). Zika virus disrupts neural progenitor development and leads to microcephaly in mice. Cell Stem Cell *19*, 672.

Lim, N.R., Shohayeb, B., Zaytseva, O., Mitchell, N., Millard, S.S., Ng, D.C.H., and Quinn, L.M. (2017). Glial-specific functions of microcephaly protein WDR62 and interaction with the mitotic kinase AURKA are essential for Drosophila Brain growth. Stem Cell Rep. *9*, 32–41.

Lin, F., Blake, D.L., Callebaut, I., Skerjanc, I.S., Holmer, L., McBurney, M.W., Paulin-Levasseur, M., and Worman, H.J. (2000). MAN1, an inner nuclear membrane protein that shares the LEM domain with lamina-associated polypeptide 2 and emerin. J. Biol. Chem. *275*, 4840–4847.

Lin, M.Y., Wang, Y.L., Wu, W.L., Wolseley, V., Tsai, M.T., Radic, V., Thornton, M.E., Grubbs, B.H., Chow, R.H., and Huang, I.C. (2017). Zika virus infects intermediate progenitor cells and post-mitotic committed neurons in human fetal brain tissues. Sci. Rep. *7*, 14883.

Liu, Y., Gordesky-Gold, B., Leney-Greene, M., Weinbren, N.L., Tudor, M., and Cherry, S. (2018). Inflammation-induced, STING-dependent autophagy restricts Zika virus infection in the Drosophila brain. Cell Host Microbe *24*, 57–68.

Lucas, E.P., and Raff, J.W. (2007). Maintaining the proper connection between the centrioles and the pericentriolar matrix requires Drosophila centrosomin. J. Cell Biol. *178*, 725–732.

Luo, L., Liao, Y.J., Jan, L.Y., and Jan, Y.N. (1994). Distinct morphogenetic functions of similar small GTPases: Drosophila Drac1 is involved in axonal outgrowth and myoblast fusion. Genes Dev. *8*, 1787–1802.

Lupski, J.R. (2015). Structural variation mutagenesis of the human genome: impact on disease and evolution. Environ. Mol. Mutagen *56*, 419–436.

Lupski, J.R., Gonzaga-Jauregui, C., Yang, Y., Bainbridge, M.N., Jhangiani, S., Buhay, C.J., Kovar, C.L., Wang, M., Hawes, A.C., Reid, J.G., et al. (2013). Exome sequencing resolves apparent incidental findings and reveals further complexity of SH3TC2 variant alleles causing Charcot-Marie-Tooth neuropathy. Genome Med. *5*, 57.

Manfruelli, P., Arquier, N., Hanratty, W.P., and Sémériva, M. (1996). The tumor suppressor gene, lethal(2)giant larvae (l(2)g1), is required for cell shape change of epithelial cells during Drosophila development. Development *122*, 2283–2294.

Marchler-Bauer, A., Bo, Y., Han, L., He, J., Lanczycki, C.J., Lu, S., Chitsaz, F., Derbyshire, M.K., Geer, R.C., Gonzales, N.R., et al. (2017). CDD/SPARCLE: functional classification of proteins via subfamily domain architectures. Nucleic Acids Res. *45*, D200–D203.

Mlakar, J., Korva, M., Tul, N., Popović, M., Poljšak-Prijatelj, M., Mraz, J., Kolenc, M., Resman Rus, K., Vesnaver Vipotnik, T., Fabjan Vodušek, V., et al. (2016). Zika virus associated with microcephaly. N. Engl. J. Med. *374*, 951–958.

Moore, C.A., Staples, J.E., Dobyns, W.B., Pessoa, A., Ventura, C.V., Fonseca, E.B., Ribeiro, E.M., Ventura, L.O., Neto, N.N., Arena, J.F., et al. (2017). Characterizing the pattern of anomalies in congenital Zika syndrome for pediatric clinicians. JAMA Pediatr. *171*, 288–295.

Nagarkar-Jaiswal, S., DeLuca, S.Z., Lee, P.T., Lin, W.W., Pan, H., Zuo, Z., Lv, J., Spradling, A.C., and Bellen, H.J. (2015a). A genetic toolkit for tagging intronic MiMIC containing genes. ELife *4*, 08469.

Nagarkar-Jaiswal, S., Lee, P.T., Campbell, M.E., Chen, K., Anguiano-Zarate, S., Gutierrez, M.C., Busby, T., Lin, W.W., He, Y., Schulze, K.L., et al. (2015b). A library of MiMICs allows tagging of genes and reversible, spatial and temporal knockdown of proteins in Drosophila. ELife *4*, 05338.

Najmabadi, H., Hu, H., Garshasbi, M., Zemojtel, T., Abedini, S.S., Chen, W., Hosseini, M., Behjati, F., Haas, S., Jamali, P., et al. (2011). Deep sequencing reveals 50 novel genes for recessive cognitive disorders. Nature *478*, 57–63.

Nam, S.C., Mukhopadhyay, B., and Choi, K.W. (2007). Antagonistic functions of Par-1 kinase and protein phosphatase 2A are required for localization of Bazooka and photoreceptor morphogenesis in Drosophila. Dev. Biol. *306*, 624–635.

Nguyen, T., Biliciler, S., Wiszniewski, W., and Sheikh, K. (2015). Expanding Phenotype of VRK1 Mutations in Motor Neuron Disease. J. Clin. Neuromuscul. Dis. *17*, 69–71.

Nichols, R.J., and Traktman, P. (2004). Characterization of three paralogous members of the mammalian vaccinia related kinase family. J. Biol. Chem. *279*, 7934–7946.

Ogawa, H., Ohta, N., Moon, W., and Matsuzaki, F. (2009). Protein phosphatase 2A negatively regulates aPKC signaling by modulating phosphorylation of Par-6 in Drosophila neuroblast asymmetric divisions. J. Cell Sci. *122*, 3242–3249.

Oláhová, M., Yoon, W.H., Thompson, K., Jangam, S., Fernandez, L., Davidson, J.M., Kyle, J.E., Grove, M.E., Fisk, D.G., Kohler, J.N., et al. (2018). Biallelic mutations in ATP5F1D, which encodes a subunit of ATP synthase, cause a metabolic disorder. Am. J. Hum. Genet. *102*, 494–504.

Peng, C.Y., Manning, L., Albertson, R., and Doe, C.Q. (2000). The tumour-suppressor genes lgl and dlg regulate basal protein targeting in Drosophila neuroblasts. Nature *408*, 596–600.

Petronczki, M., and Knoblich, J.A. (2001). DmPAR-6 directs epithelial polarity and asymmetric cell division of neuroblasts in Drosophila. Nat. Cell Biol. *3*, 43–49.

Port, F., Chen, H.M., Lee, T., and Bullock, S.L. (2014). Optimized CRISPR/Cas tools for efficient germline and somatic genome engineering in Drosophila. Proc. Natl. Acad. Sci. USA *111*, E2967–E2976.

Posey, J.E., O'Donnell-Luria, A.H., Chong, J.X., Harel, T., Jhangiani, S.N., Coban Akdemir, Z.H., Buyske, S., Pehlivan, D., Carvalho, C.M.B., Baxter, S., et al. (2019). 'Insights into genetics, human biology and disease gleaned from family based genomic studies'. Copy number variant and runs of homozygosity detection by microarrays enabled more precise molecular diagnoses in 11,020 clinical exome cases. Genet. Med. *11*, 30.

Poulton, J.S., Cuningham, J.C., and Peifer, M. (2017). Centrosome and spindle assembly checkpoint loss leads to neural apoptosis and reduced brain size. J. Cell Biol. *216*, 1255–1265.

Ramdas Nair, A., Singh, P., Salvador Garcia, D., Rodriguez-Crespo, D., Egger, B., and Cabernard, C. (2016). The microcephaly-associated protein Wdr62/CG7337 is required to maintain centrosome asymmetry in Drosophila neuroblasts. Cell Rep. *14*, 1100–1113.

Reid, J.G., Carroll, A., Veeraraghavan, N., Dahdouli, M., Sundquist, A., English, A., Bainbridge, M., White, S., Salerno, W., Buhay, C., et al. (2014). Launching genomics into the cloud: deployment of mercury, a next generation sequence analysis pipeline. BMC Bioinformatics *15*, 30.

Renbaum, P., Kellerman, E., Jaron, R., Geiger, D., Segel, R., Lee, M., King, M.C., and Levy-Lahad, E. (2009). Spinal muscular atrophy with pontocerebellar hypoplasia is caused by a mutation in the VRK1 gene. Am. J. Hum. Genet. *85*, 281–289.

Riedel, F., Gillingham, A.K., Rosa-Ferreira, C., Galindo, A., and Munro, S. (2016). An antibody toolkit for the study of membrane traffic in Drosophila melanogaster. Biol. Open *5*, 987–992.

Riemer, D., Stuurman, N., Berrios, M., Hunter, C., Fisher, P.A., and Weber, K. (1995). Expression of Drosophila lamin C is developmentally regulated: analogies with vertebrate A-type lamins. J. Cell Sci. *108*, 3189–3198.

Rolls, M.M., Albertson, R., Shih, H.P., Lee, C.Y., and Doe, C.Q. (2003). Drosophila aPKC regulates cell polarity and cell proliferation in neuroblasts and epithelia. J. Cell Biol. *163*, 1089–1098.

Rujano, M.A., Sanchez-Pulido, L., Pennetier, C., le Dez, G., and Basto, R. (2013). The microcephaly protein Asp regulates neuroepithelium morphogenesis by controlling the spatial distribution of myosin II. Nat. Cell Biol. *15*, 1294–1306.

Sanger, F., Nicklen, S., and Coulson, A.R. (1977). DNA sequencing with chain-terminating inhibitors. Proc. Natl. Acad. Sci. U S A *74*, 5463–5467.

Sanz-García, M., Vázquez-Cedeira, M., Kellerman, E., Renbaum, P., Levy-Lahad, E., and Lazo, P.A. (2011). Substrate profiling of human vaccinia-related kinases identifies coilin, a Cajal body nuclear protein, as a phosphorylation target with neurological implications. J. Proteomics *75*, 548–560.

Sarov, M., Barz, C., Jambor, H., Hein, M.Y., Schmied, C., Suchold, D., Stender, B., Janosch, S., K J, V.V., Krishnan, R.T., et al. (2016). A genome-wide resource for the analysis of protein localisation in Drosophila. ELife *5*, e12068.

Schober, M., Schaefer, M., and Knoblich, J.A. (1999). Bazooka recruits Inscuteable to orient asymmetric cell divisions in Drosophila neuroblasts. Nature *402*, 548–551.

Segura-Totten, M., Kowalski, A.K., Craigie, R., and Wilson, K.L. (2002). Barrier-to-autointegration factor: major roles in chromatin decondensation and nuclear assembly. J. Cell Biol. *158*, 475–485.

Seidl, S., Braun, U., Roos, N., Li, S., Lüdtke, T.H., Kispert, A., and Leitges, M. (2013). Phenotypical analysis of atypical PKCs in vivo function display a compensatory system at mouse embryonic day 7.5. PLoS One *8*, e62756.

Shah, P.S., Link, N., Jang, G.M., Sharp, P.P., Zhu, T., Swaney, D.L., Johnson, J.R., Von Dollen, J., Ramage, H.R., Satkamp, L., et al. (2018). Comparative Flavivirus-host protein interaction mapping reveals mechanisms of dengue and Zika virus pathogenesis. Cell *175*, 1931–1945.

Shaheen, R., Maddirevula, S., Ewida, N., Alsahli, S., Abdel-Salam, G.M.H., Zaki, M.S., Tala, S.A., Alhashem, A., Softah, A., Al-Owain, M., et al. (2019). Genomic and phenotypic delineation of congenital microcephaly. Genet. Med. *21*, 545–552.

Shinawi, M., Liu, P., Kang, S.H., Shen, J., Belmont, J.W., Scott, D.A., Probst, F.J., Craigen, W.J., Graham, B.H., Pursley, A., et al. (2010). Recurrent reciprocal 16p11.2 rearrangements associated with global developmental delay, behavioural problems, dysmorphism, epilepsy, and abnormal head size. J. Med. Genet. *47*, 332–341.

Siller, K.H., Cabernard, C., and Doe, C.Q. (2006). The NuMA-related Mud protein binds Pins and regulates spindle orientation in Drosophila neuroblasts. Nat. Cell Biol. *8*, 594–600.

Smith, A.C., McGavran, L., Robinson, J., Waldstein, G., Macfarlane, J., Zonona, J., Reiss, J., Lahr, M., Allen, L., and Magenis, E. (1986). Interstitial deletion of (17)(p11.2p11.2) in nine patients. Am. J. Med. Genet. *24*, 393–414.

Snyers, L., Erhart, R., Laffer, S., Pusch, O., Weipoltshammer, K., and Schöfer, C. (2018). LEM4/ANKLE-2 deficiency impairs post-mitotic re-localization of BAF, LAP2α and lamina to the nucleus, causes nuclear envelope instability in telophase and leads to hyperploidy in HeLa cells. Eur. J. Cell Biol. *97*, 63–74.

Soloff, R.S., Katayama, C., Lin, M.Y., Feramisco, J.R., and Hedrick, S.M. (2004). Targeted deletion of protein kinase C lambda reveals a distribution of functions between the two atypical protein kinase C isoforms. J. Immunol. *173*, 3250–3260.

Stoll, M., Teoh, H., Lee, J., Reddel, S., Zhu, Y., Buckley, M., Sampaio, H., Roscioli, T., Farrar, M., and Nicholson, G. (2016). Novel motor phenotypes in

patients with VRK1 mutations without pontocerebellar hypoplasia. Neurology *87*, 10.1212/WNL.0000000000002813.

Summerville, J.B., Faust, J.F., Fan, E., Pendin, D., Daga, A., Formella, J., Stern, M., and McNew, J.A. (2016). The effects of ER morphology on synaptic structure and function in Drosophila melanogaster. J. Cell Sci. *129*, 1635–1648.

Suzuki, A., and Ohno, S. (2006). The PAR-aPKC system: lessons in polarity. J. Cell Sci. *119*, 979–987.

Tang, H., Hammack, C., Ogden, S.C., Wen, Z., Qian, X., Li, Y., Yao, B., Shin, J., Zhang, F., Lee, E.M., et al. (2016). Zika virus infects human cortical neural progenitors and attenuates their growth. Cell Stem Cell *18*, 587–590.

Venken, K.J., Carlson, J.W., Schulze, K.L., Pan, H., He, Y., Spokony, R., Wan, K.H., Koriabine, M., de Jong, P.J., White, K.P., et al. (2009). Versatile P[acman] BAC libraries for transgenesis studies in Drosophila melanogaster. Nat. Methods *6*, 431–434.

Venken, K.J., He, Y., Hoskins, R.A., and Bellen, H.J. (2006). P[acman]: a BAC transgenic platform for targeted insertion of large DNA fragments in D. melanogaster. Science *314*, 1747–1751.

Venken, K.J., Kasprowicz, J., Kuenen, S., Yan, J., Hassan, B.A., and Verstreken, P. (2008). Recombineering-mediated tagging of Drosophila genomic constructs for in vivo localization and acute protein inactivation. Nucleic Acids Res. *36*, e114.

Venken, K.J., Schulze, K.L., Haelterman, N.A., Pan, H., He, Y., Evans-Holm, M., Carlson, J.W., Levis, R.W., Spradling, A.C., Hoskins, R.A., et al. (2011). MiMIC: a highly versatile transposon insertion resource for engineering Drosophila melanogaster genes. Nat. Methods *8*, 737–743.

Wang, C., Chang, K.C., Somers, G., Virshup, D., Ang, B.T., Tang, C., Yu, F., and Wang, H. (2009). Protein phosphatase 2A regulates self-renewal of Drosophila neural stem cells. Development *136*, 2287–2296.

Wang, H., Ouyang, Y., Somers, W.G., Chia, W., and Lu, B. (2007). Polo inhibits progenitor self-renewal and regulates Numb asymmetry by phosphorylating Pon. Nature *449*, 96–100.

Wang, H., Somers, G.W., Bashirullah, A., Heberlein, U., Yu, F., and Chia, W. (2006). Aurora-A acts as a tumor suppressor and regulates self-renewal of Drosophila neuroblasts. Genes Dev. *20*, 3453–3463.

Wirtz-Peitz, F., Nishimura, T., and Knoblich, J.A. (2008). Linking cell cycle to asymmetric division: Aurora-A phosphorylates the Par complex to regulate Numb localization. Cell *135*, 161–173.

Wodarz, A., Hinz, U., Engelbert, M., and Knust, E. (1995). Expression of crumbs confers apical character on plasma membrane domains of ectodermal epithelia of Drosophila. Cell *82*, 67–76.

Wu, N., Ming, X., Xiao, J., Wu, Z., Chen, X., Shinawi, M., Shen, Y., Yu, G., Liu, J., Xie, H., et al. (2015). TBX6 null variants and a common hypomorphic allele in congenital scoliosis. N. Engl. J. Med. *372*, 341–350.

Yakulov, T., Günesdogan, U., Jäckle, H., and Herzig, A. (2014). Bällchen participates in proliferation control and prevents the differentiation of Drosophila melanogaster neuronal stem cells. Biol. Open *3*, 881–886.

Yamamoto, S., Jaiswal, M., Charng, W.L., Gambin, T., Karaca, E., Mirzaa, G., Wiszniewski, W., Sandoval, H., Haelterman, N.A., Xiong, B., et al. (2014). A Drosophila genetic resource of mutants to study mechanisms underlying human genetic diseases. Cell *159*, 200–214.

Zhong, W., Jiang, M.M., Schonemann, M.D., Meneses, J.J., Pedersen, R.A., Jan, L.Y., and Jan, Y.N. (2000). Mouse numb is an essential gene involved in cortical neurogenesis. Proc. Natl. Acad. Sci. U S A *97*, 6844–6849.

STAR★METHODS

KEY RESOURCES TABLE

REAGENT or RESOURCE	SOURCE	IDENTIFIER
Antibodies		
Anti-Deadpan (Rat) 11D1CH11	Abcam	Cat#ab19517
Anti-Prospero MR1A (Mouse)	Developmental Studies Hybridoma Bank	RRID: AB_528440
Anti-Miranda (Rat)	Abcam	Cat#ab197788
Anti-aPKC (Rabbit) PKCz (C-20)	Santa Cruz, discontinued	RRID: AB_2300359
Anti-GFP (Rabbit)	Invitrogen	Cat#A11122; RRID AB_221569
Anti-Calnexin 99a (Mouse) 6-2-1	Developmental Studies Hybridoma Bank	Cat#Cnx99A 6-2-1; RRID: AB_2722011
Anti-Bazooka (Guinea Pig)	Siller et al., 2006	N/A
Anti-Par6 (Rat)	Rolls et al., 2003	N/A
Anti-Phospho-Histone H3 (Rabbit) Ser10	Millipore	Cat#06–570; RRID: AB_310177
Anti-Ball (Rabbit)	Yakulov et al., 2014	RRID: AB_2567974
Anti-VRK1 (Rabbit) EPR10623(B)	Abcam	Cat#ab151706
Anti-Cnn (Rabbit)	Lucas and Raff, 2007	N/A
Anti-Strep (Mouse)	Qiagen	Cat#34850
Anti-aPKC (Rabbit) phosphoT410	Santa Cruz, discontinued	N/A
Anti-Actin-c4 (Mouse)	Millipore	Cat#MAB1501; RRID: AB_2223041
Anti–L(2)Gl (Rat)	Peng et al., 2000	RRID: AB_2569164
Donkey Anti-Rat-Cy3	Jackson ImmunoResearch	Cat#112-165-167; RRID: AB_2338251
Donkey Anti-rabbit-488	Jackson ImmunoResearch	Cat#711-545-152; RRID: AB_2313584
Donkey Anti-Mouse-Cy5	Jackson ImmunoResearch	Cat#715-605-151; RRID: AB_2340863
Anti-Rabbit-DyLight800	Rockland	Cat#611-145-002; RRID: AB_1660964
Anti-Rat-DyLight 680	Rockland	Cat#612-144-002; RRID: AB_11181430
Anti-Rabbit Peroxidase	Jackson ImmunoResearch	Cat#111-035-144; RRID: AB_2307391
Experimental Models: Cell Lines		
Human Primary Fibroblast Culture ANKLE2 p.L573V/+	This study	N/A
Human Primary Fibroblast Culture ANKLE2 p.L573V/p.Q782*	This study	N/A
Human Primary Fibroblast Culture ANKLE2 p.V229G/p.V229G	This study	N/A
Experimental Models: Organisms/Strains		
D.melanogaster FRT19a	Yamamoto et al., 2014	N/A
D.melanogaster Ankle2^{A}	Yamamoto et al., 2014	N/A
D.melanogaster Ankle2^{CRIMIC}	This study	N/A
D.melanogaster Ankle2^{IGFP}	This study	N/A
D.melanogaster Ankle2-GFPR	This study	N/A
D.melanogaster P{UASt- hANKLE2}VK37	Yamamoto et al., 2014	N/A
D.melanogaster P{UASt-hANKLE2 p.L537V }VK37	This study	N/A
D.melanogaster P{UASt-hANKLE2 p.Q782}VK37*	This study	N/A
D.melanogaster P{UASt-hANKLE2 p.A109P}VK37	This study	N/A
D.melanogaster P{UASt-hANKLE2 p.G201W}VK37	This study	N/A
D.melanogaster P{20XUAS-tdTomato-Sec61beta}attP2	Summerville et al., 2016	BDSC: 64747
D.melanogaster ball^{e107}	Cullen et al., 2005	N/A
D.melanogaster Ball^{2}	Herzig et al., 2014	N/A

(*Continued on next page*)

Continued

REAGENT or RESOURCE	SOURCE	IDENTIFIER
D.melanogaster l(2)gIMI07575-GFSTF.0	Nagarkar-Jaiswal et al., 2015a	BDSC: 63183
D.melanogaster l(2)gl^{ts3}cn^{1}sp^{13}	Manfruelli et al., 1996	BDSC: 63183
D.melanogaster P{UASt-NS4Aug}	Shah et al., 2018	N/A
D.melanogaster PGW{UAS-NS4Aug-HA}	This study	N/A
D.melanogaster P{UASt-mCD8-GFP}	Lee and Luo, 2001	BDSC: 5137
D.melanogaster Actin-GAL4 (P{Act5C-GAL4}17bFO1)	Ito et al., 1997	BDSC: 3954
D.melanogaster Actin-GAL4 (P{Act5C-GAL4}25FO1)	Ito et al., 1997	BDSC: 4414
D.melanogaster inscuteable-GAL4 (P{w[+mW.hs]=GawB}insc[Mz1407])	Luo et al., 1994	BDSC: 8751
D.melanogaster Daughterless-GAL4 (P{w[+mW.hs]=GAL4-da.G32}UH1)	Wodarz et al., 1995	BDSC: 55850
D.melanogaster Ball-GFP (fTRG-823)	Sarov et al., 2016	N/A
D.melanogaster wor-mira-cherry P{w[+mC]=wor. GAL4.A}2,P{w[+mC]=UAS-mira.cherry}2/CyO)	Cabernard and Doe, 2009	BDSC: 56556
D.melanogaster P{His2Av[T:Avic\GFP-S65T]}62A	Clarkson and Saint, 1999	BDSC: 5941
D.melanogaster P{w[+mC]=UAS-aurA.Exel}2	BDSC	BDSC: 8377
D.melanogaster M{UAS-aPKC.ORF.3xHA}ZH-86Fb	Bischof et al., 2013	FlyORF: F000876
D.melanogaster P{w[+mC]=UAS-aPKC.DeltaN}3	Drier et al., 2002	BDSC: 51673
D.melanogaster w;attP40(y+){Nos-Cas9(v+)}/CyO	Kondo and Ueda, 2013	N/A
Oligonucleotides		
Ankle2 gRNA1: ATAAAGTATTTTCTTAACGGTGG	This study	N/A
Ankle2 gRNA2: TAATAATTTTAAATTCTCATTGG	This study	N/A
Ankle2LAF:ccatagctatggGCAATTCCTCAATGTC GAATTTACTGCTCA	This study	N/A
Ankle2LAR:ttatgcatATTTTCTTAACGGTGGGA AATTATAC	This study	N/A
Ankle2RAF:agcatgcATACTTTATTATTGCATTT GTTATAAGTATGAGA	This study	N/A
Ankle2RAR:tactcgagGCAAAGTTCCAGACCGT TTCTGATTTATC	This study	N/A
GFP1:GGGATCAACGGTCCTATAACGAGGGGG ACACGCCGCTGGGCAATCGGAAC GCAGCCCAATTCCGATCATATTC	This study	N/A
GFP2:CATCAATCAGTCGCTGTTTCTGTTTCTG TTTCCGGGCCGATT CCGTTTCA TTACTTGTACAGCTCGTCCATG	This study	N/A
Recombinant DNA		
BAC CH321-85N12	Venken et al., 2009 BACPAC Resources	N/A
Software and Algorithms		
Mercury Pipeline, DNANexus	Reid et al., 2014	http://blog.dnanexus.com/2013-10-22-run-mercury-variant-calling-pipeline
Data and Code Availability		
Exome sequence	Gonzaga-Jauregui et al., 2012	dbGaP: phs000711.v5.p1

LEAD CONTACT AND MATERIALS AVAILABILITY

All unique/stable reagents generated in this study are available from the Lead Contact without restriction. Further information and requests for resources and reagents should be directed to and will be fulfilled by the Lead Contact, Hugo J. Bellen (hbellen@bcm.edu).

EXPERIMENTAL MODEL AND SUBJECT DETAILS

Drosophila melanogaster

The following fly lines were used: *FRT19a* (Yamamoto et al., 2014), *Ankle2*^{A} (Yamamoto et al., 2014), *Ankle2*^{CRIMIC} (this study), *Ankle2*^{IGFP}(this study), *Ankle2-GFPR* (this study), *P{UASt- hANKLE2}VK37* (Yamamoto et al., 2014), *P{UASt-hANKLE2 p.L537V }VK37* (this study), *P{UASt-hANKLE2 p.Q782*}VK37* (this study), *P{UASt-hANKLE2 p.A109P}VK37* (this study), *P{UASt-hANKLE2 p.G201W}VK37* (this study), *P{20XUAS-tdTomato-Sec61beta}attP2* (Summerville et al., 2016), *ball*^{e107}(Cullen et al., 2005), *ball*^{2} (Herzig et al., 2014), *l(2)gIMI07575-GFSTF.0* (Nagarkar-Jaiswal et al., 2015a), *l(2)gl*^{ts3}*cn*^{1}*sp*^{13} (Manfruelli et al., 1996), *P{UASt-NS4Aug}* (Shah et al., 2018), *P{GW UAS-NS4Aug-HA}* (this study), *P{UASt-CD8-GFP}* (Lee and Luo, 2001), *actin-GAL4* (*P{Act5C-GAL4} 17bFO1*) (Ito et al., 1997), *inscuteable-GAL4* (*P{w[+mW.hs]=GawB}insc[Mz1407]*) (Luo et al., 1994), *daughterless-GAL4 (P{w [+mW.hs]=GAL4-da.G32}UH1)* (Wodarz et al., 1995), *ball-GFP (fTRG-823)* (Sarov et al., 2016), *wor-mira-cherry P{w[+mC]=wor.-GAL4.A}2,P{w[+mC]=UAS-mira.cherry}2/CyO)* (Cabernard and Doe, 2009), *P{His2Av[T:Avic\GFP-S65T]}62A* (Clarkson and Saint, 1999), *P{w[+mC]=UAS-aurA.exel}2*, *M{UAS-aPKC.ORF .3xHA}ZH-86Fb* (Bischof et al., 2013), *P{w[+mC]=UAS-aPKC.deltan}3* (Drier et al., 2002). All flies were maintained at 22°C and grown on standard cornmeal and molasses medium in plastic vials. Crosses were performed at temperature indicated (18°C, 22°C, 25°C, or 29°C). Hemizygous males were analyzed as *Ankle2* mutants (which is on the X chromosome) and females were used for *Ankle2* heterozygous studies. All other studies contained males and females. Brain volume measurements were conducted in late 3rd instar larvae (gut clearance, extruding spiracles). *Act-GAL4* was use to ubiquitously express Zika virus NS4A and Sec61β, *da-GAL4* was used to express human ANKLE2 constructs and aPKC, *insc-GAL4* was used to express NS4A in neuroblasts.

Human Studies

All study subjects enrolled into the Baylor-Hopkins Center for Mendelian Genomics (BHCMG) provided informed consent for exome sequencing and study participation under the Baylor College of Medicine Institutional Review Board-approved protocol H-29697. BAB701 provided informed consent for molecular and genomic analysis under the Baylor College of Medicine Institutional Review Board-approved protocol H-9170. All study subjects enrolled through Baylor Genetics Laboratory (BGL) were analyzed on a retrospective basis, and only de-identified information is provided under the Baylor College of Medicine Institutional Board approved protocol H-41191. Patients were ascertained from the 7148 sequenced individuals in BHCMG or the ~12500 sequenced individuals in the BGL by searching for biallelic variants with CADD scores >15 in conjunction with phenotypes of interest. Six male and two female patients were ascertained from the BHCMG database. The age of the patient is known for 3 individuals (2y, 7y, 32y). Two female and three male patients were ascertained from the BGL database. Ages at referral were 2 months, 7y, 12y, 20y, and 41y.

Human Clinical Information

BAB4821

A homozygous missense variant in *VRK2* (c.1234G>A;p.D412N; Table S2; Figure S6) was observed in a proband, BAB4821 born to consanguineous Turkish parents, with nanophthalmos. The variant was in a region of absence of heterozygosity (AOH) ~7.7Mb in length gleaned from unphased ES data (Karaca et al., 2018) and consistent with identity-by-descent.

BAB7812

In BAB7812, a patient with severe microcephaly (Z score = -6.7) and additional brain malformations including cortical dysplasia and agenesis of the corpus callosum, a homozygous variant with a predicted detrimental effect on splicing in a canonical splice site within *VRK3* (c.139+2 T>G) was found (Table S2; Figure S6). Additional homozygous variants were found in the same (*PNKP*) and an adjacent (*RNT2*) AOH block as *VRK3* (Table S2; Figure S6). All three homozygous variants are predicted deleterious. *PNKP* has a known disease association with microcephaly, seizures, and developmental delay (MIM#613402) while *RNT2* has a known disease association with Spastic paraplegia 12 (MIM#604805). Multilocus variation may contribute to the phenotype in BAB7812. The proband was born full term to consanguineous Turkish parents. At 5 months of age, he developed seizures. At 32 months, he was unable to walk, and his weight was 9.8kg (-3.34SD), height was 85cm (-2.03SD), and head circumference was 36.7cm (-6.7SD). Physical examination revealed thick eyebrows, protuberant ears, and almond shaped eyes. Metabolic and ocular examinations were within normal limits. He received continued follow-up care for microcephaly and refractory epilepsy, and special education for associated intellectual disability and developmental delay. His occipital frontal circumference was below the 3rd percentile when measured at 8–11 years of age. Parents and an unaffected sibling were heterozygous for the variant, demonstrating segregation of the variant with disease.

BAB10531

A BHCMG search database found a homozygous predicted deleterious missense variant in *PARD3B* (c.1222G>A, p.G408S) in BAB10531 who has microcephaly (Table S2; Figure S6). At 15 months, weight he was 9kg (-2.1SD), height was 79cm (0.4SD), and head circumference was 44.5cm (Z = -2.2 measured at 15m and and 18m). Both unaffected consanguineous parents of Turkish descent were heterozygous for the variant that mapped to a region of AOH ~22Mb in length. BAB10531 has had frequent upper respiratory tract infections and was admitted at 17 months of age to investigate a cause for with no clear etiology found. Follow-up head circumference was performed at 18 months, which demonstrated microcephaly was non-progressive (45cm, -2.2SD). Notably, no follow-up for intellectual disability was described on recruitment to the BHCMG.

BAB8223

In BAB8223, a proband with distal arthrogryposis, a homozygous missense variant in *PARD3B* (c.1654G>A;p.A552T) which segregated with disease was found (Table S2; Figure S6). The proband was born to consanguineous Turkish parents and the homozygous variant was found within a region of AOH ~37Mb in length. At age 5.5y head circumference was 49cm (13th percentile, ~ -1SD). Cognitive and motor development is within normal limits.

BGL – 1

Referral diagnosis: microcephaly, intrauterine growth restriction, radial microbrain and immature gyral pattern.

BGL – 2

Referral diagnosis: global developmental delay with aphasia, microcephaly and seizures, progressive weakness, lethargy with episodes of irregular breathing and respiratory acidosis, MRI showing progressive diffuse central white matter atrophy and gliosis, hypomyelination, atrophy of thalami and pons. (Table S2; Figure S2)

BGL – 3

Referral diagnosis: intellectual disability, ataxia, spasticity, autism spectrum disorder, speech delay, and anxiety disorder. (Table S2; Figure S2)

BGL – 4

Referral diagnosis: spinal muscular atrophy complicated by failure to thrive and respiratory insufficiency, microcephaly, short stature, scoliosis, delayed motor milestones, progressive weakness, hypotonia, history of prematurity and intrauterine growth retardation (Table S2; Figure S5).

BGL – 5

Referral diagnosis: prematurity, spasticity of inferior limbs, seizures, contractures of the Achilles, myopia (Table S2; Figure S5).

Human Primary Cultures

Fibroblasts were cultured in flasks containing Gibco DMEM (1x) with 4.5g/L D-glucose, L-glutamine, 25mM HEPES, HyClone FBS (10%), and Gibco Anti-Anti (1%) at 37 degrees Celsius with 5% CO_2. Cultures of p.L573V/+ and p.L573V/p.Q782* were male; p.V229G/p.V229G was female.

METHOD DETAILS

Generation of Ankle2 Mutations and Constructs

To generate *Ankle2*^{CRIMIC} by CRISPR-Cas9, two guide RNAs targeting *Ankle2*, 5′-ATAAAGTATTTTCTTAACGGTGG-3′ and 5′-TAA TAATTTTAAATTCTCATTGG-3′ with PAM sites underlined , were cloned into pCDF3 (Port et al., 2014). Regions of homology targeting the 4th coding intron were cloned into PM14 (Lee et al., 2018) using 5′- ccatagctatggGCAATTCCTCAATGTCGAATTTACTGCTCA-3′ and 5′- ttatgcatATTTTCTTAACGGTGGGAAATTATAC-3′ to amplify the left arm for BstXI/NsiI cloning and 5′- tagcatgcATACTTTAT TATTGCATTTGTTATAAGTATGAGA-3′ and 5′- tactcgagGCAAAGTTCCAGACCGTTTCTGATTTATC-3′ to amplify the right arm for conventional cloning with SphI/XhoI. This donor construct and two guide RNA constructs were injected into *,w;attP40(y+){nos-Cas9(v+)}/CyO* (Kondo and Ueda, 2013) embryos, and positive expression of *3XP3-GFP* was used to isolate animals with targeted events. PCR and genomic sequencing of surrounding regions validated the *Ankle2*^{CRIMIC} allele. *Ankle*^{IGFP} was generated by RMCE by injecting a plasmid expressing integrase with pBS-KS-attB1-2-PT-SA-SD-EGFP-FlAsH-StrepII-TEV-3xFlag (Nagarkar-Jaiswal et al., 2015b) into *Ankle2*^{CRIMIC} animals. Animals with 3XP3-GFP loss were screened using PCR for targeted cassette exchange. Regions flanking the targeted event were sequenced to verify the allele. The *Ankle2-GFPR* was created using recombineering (Venken et al., 2008) of BAC CH321-85N12 (Venken et al., 2006). A GFP donor construct was generated by amplifying the GFP coding region and a selection cassette from plasmid PL-452 C-EGFP with primers containing 50bp homology with the C-terminal end of Ankle2 (5'-GGGATCAACGGTCCTATAACGAGGGGGACACGCCGCTGGGCAATCGGAACGCAGCCCAATTCCGATCATATTC-3' and 5'-CAT CAATCAGTCGCTGTTTCTGTTTCTGTTTCCGGGCCGATT CCGTTTCATTACTTGTACAGCTCGTCCATG-3'. Regions matching PL-452 C-EGFP are underlined. CH321-85N12 was transformed into DY380 cells using electroporation. Stable colonies were grown overnight at 30°C, induced for recombination functions at 42°C for 15 min, and transformed using electroporation (1.8kV, 200Ohm, 25μFD) with the amplified donor construct. Colonies were selected for both the BAC (chloramphenicol) and insertion of GFP (kanamycin). Resulting colonies were verified using PCR, restriction enzyme digestion, and sequencing. The GFP tag selection cassette was removed using Cre mediated excision by transforming the *Ankle2-GFP* BAC into induced EL350 cells. Properly excised events were verified by PCR, absence of growth on kanamycin selection plates, and sequencing.

Generation of Human ANKLE2 and NS4A-HA Expression Constructs

NEB Q5 Site-directed mutagenesis was performed on *P{UASt- hANKLE2}*. Each plasmid was sequence verified and injected into VK37 flies with a plasmid expressing integrase for site-specific integration. NS4A, including the 2K peptide, from strain MR-766 was PCR amplified from UASt-NS4A (Shah et al., 2018) and Gibson assembly was used to insert NS4A into pGW-HA.attB linearized with AgeI and KpnI to remove the ccdB region. Resulting vector was injected into VK37 flies as above.

Brain Immunostaining

Late 3rd instar (based on gut clearance and extruding spiracles) larval brains were dissected in PBS and fixed with 4% PFA/PBS/0.3% Triton for 20 minutes. For immunostaining, brains were blocked in PBS/0.3%Triton/1%BSA/5% normal goat serum and incubated in primary antibody in PBS/0.3%Triton/1%BSA overnight. Primary antibodies include rat anti-Deadpan (Abcam Cat# ab195172, 1:250 or 1:500), mouse anti-Prospero MR1A (Developmental Studies Hybridoma Bank, 1:1000), rat anti-Miranda (1:500, Abcam Cat# ab197788), rabbit anti-aPKC (1:1000, PKCz (C-20) Santa Cruz, discontinued), rabbit anti-GFP (1:1000, Invitrogen Cat# A11122), mouse anti-calnexin 99a (Developmental Studies Hybridoma Bank, 1:100), mouse anti-Lamin Dm0 ADL67.10 (Developmental Studies Hybridoma Bank, 1:250), guinea pig anti-Bazooka (1:1000) (Siller et al., 2006), rat anti-Par-6 (1:50) (Rolls et al., 2003), rabbit anti-phospho-histone H3 (1:1000, Millipore Cat# 06–570), rabbit anti-Ball (1:1000) (Yakulov et al., 2014), rabbit anti-VRK1 (1:1000, Abcam Cat# ab151706), rabbit anti-Cnn (1:1000) (Lucas and Raff, 2007), and mouse anti-Strep (Qiagen Cat# 34850, 1:500) with goat or donkey secondary antibodies from Jackson ImmunoResearch used 1:500. Brains were mounted with double sided tape spacers and imaged using a Leica Sp8 with 2 μm or 3 μm sections through the entire brain lobe.

Live Imaging

3rd instar larvae were dissected in sterile PBS supplemented with 1% FBS and 0.5mM ascorbic acid, fine dissected on an inverted Sarstedt lumox dish 50 in a petroleum jelly well. Samples were imaged on a Leica Sp8 with optimized settings for high quality images without bleaching or a Zeiss 880 with Airy scan (wild type Ankle2-GFP and Sec61β colocalization).

Protein Immunoprecipitation and Western Analysis

3rd instar larvae or dissected larval brains from *l(2)gl*$^{MI07575\text{-}GFSTF.0}$ animals were dissociated in 0.1% CHAPS buffer supplemented with protease and phosphatase inhibitors for at least 30 min on ice, centrifuged for 10 min at 4°C, and supernatant was used for immunoprecipitation or western analysis. For immunopreciptation, 25μl of Allele Biotechnology GFP nanoantibody agarose (nAb, Cat# ABP-NAB-GFPA100) was equilibrated and incubated with lysate 2hrs - overnight at 4°C with rotation. Agarose was spun down for 1 min at 1000 × *g* at 4°C, supernatant was removed, and pellet was washed 3X (1× binding buffer (10mM Tris-HCl pH 7.5,150mM NaCl), 2× wash buffer (10mM Tris-HCl pH7.5, 500mM NaCl)). Remaining agarose pellet was eluted for western analysis in loading buffer. For western analysis, larval brains were dissected and dissociated as stated above, and were lysed in 0.1% CHAPS buffer [[50mM NaCl, 200mM HEPES, 1mM EDTA and protease inhibitor cocktail (Roche)] Loading input was adjusted for brain size and protein concentration. Primary antibodies include rabbit anti-GFP (1:2500, Invitrogen Cat# A11122), rabbit anti-Ball (1:1000) (Herzig et al., 2014), rat anti-L(2)gl (Peng et al., 2000), rabbit anti-aPKC c-20 (1:1000, Santa Cruz, discontinued), rabbit anti-aPKC phosphoT410 (1:1000, Santa Cruz, discontinued), and mouse anti-actin-c4 (1:5000, Millipore Cat# MAB1501). Secondary antibodies include Rockland DyLight 600 and 800 (1:1000), BioRad Star Bright Blue 700 (1:1000) and Jackson ImmunoResearch HRP conjugated (1:5000). Blots were imaged on a Bio-Rad ChemiDocMP.

Food Ingestion Assay

Ankle^{2}*A/Y or Ankle2*^{A}/+ third instar lavae from the same vial were washed in PBS and placed on yeast paste containing 0.08% Brilliant Blue R dye in 10mm petri dishes for 20 minutes. Larvae were transferred, rinsed, boiled for 10 sec, and aligned on a glass slide ventral side up. Larvae from both genotypes were imaged at the same time using a Biorad ChemiDoc MP Imaging system using the 715/30 (far red/680) filter. Total intensity of blue food in the gut was measured using Biorad's ImageLab software and plotted as total intensity per lavae.

Human Cell Immunohistochemistry

Cells were detached using trypsin-EDTA 0.05% and plated onto 18-mm glass cover slips in 6 well plates. Cells were cultured for an additional 3 days under the same conditions before fixing and staining. Cells were rinsed with PBS followed by fixing in 4% paraformaldehyde in PBS. Cells were rinsed and washed 3× in PBST, washed 2× in PBST + 1% BSA (PBSTB), and then blocked in PBSTB + 5% normal goat serum. They were then incubated in PBSTB and primary antibody overnight at 4 degrees Celsius. Cells were then washed 3× in PBSTB, incubated in anti-rabbit Cy5 secondary antibody (1:500) for 2 hours, and washed 3× in PBST. The cells were given a final wash in PBST with DAPI (1:1000) for 30m before mounting using SlowFade glow on glass slides and sealing with nail polish.

Exome and Sanger Sequencing

Exome sequencing was performed under the Baylor Hopkins Center for Mendelian Genomics (BHCMG) research initiative as previously described (Lupski et al., 2013). Exome capture was performed with Nimblegen reagents and a custom capture reagent, VCRome2.1. Raw data was processed using the Mercury variant calling pipeline, available on DNANexus. http://blog.dnanexus.com/2013-10-22-run-mercury-variant-calling-pipeline/ (Reid et al., 2014) and the ATLAS2 method was used for variant calling followed by an in-house Cassandra annotation pipeline based on Annotation of Genetic Variants (ANNOVAR). The *LLGL1* variant was orthogonally validated and segregated with disease by dideoxy Sanger sequencing of PCR amplicons (Sanger et al., 1977).

QUANTIFICATION AND STATISTICAL ANALYSIS

Brain Volume

Brains from third instar larvae were stained and mounted with tape spacers and imaged using a Leica Sp8 with 2 μm or 3 μm sections through the entire brain lobe. Resulting stacks were analyzed using the Surfaces function in Imaris (Bitplane) to quantify brain lobe volume as total microns cubed. One lobe from each brain was imaged and a total of 5–10 brains were analyzed per genotype or condition. Brain lobe volumes are displayed as box plots with hinges representing the 25^{th} to 75^{th} percentiles, a line represents the median, and whiskers represent min to max. Statistical significance was determined using one-way ANOVA with multiple comparisons post-test calculated using GraphPad Prism. Brain volumes in Figure 1 are normalized to wild type (*FRT19a*). Average volume from wild type is set to 100%, and each mutant or condition is normalized as percentage of wild type volume. Brain volumes from Figures 4 and 5 are displayed as total brain volume (μm^3).

Asymmetric Phenotypes

3^{rd} instar larvae were immunostained for pH3, Baz, Par-6, aPKC, or Mira as described above. Metaphase neuroblasts (pH3 positive, chromosomes aligned at the metaphase plate) were imaged on a Leica Sp8 (63X). Only metaphase neuroblasts in the correct plane for imaging were analyzed. Mild disruption refers to weak or incomplete crescent localization, and strong disruption indicates no crescent localization. To quantify spindle orientation, Cnn was used to mark the plane of division, and aPKC, and Mira were used to establish cortex polarity. Only metaphase neuroblasts in the correct plane for imaging were analyzed. The angle between spindle orientation and cortex polarity was measured using the angle function of ImageJ. Phenotypes are portrayed as percentage of total counted metaphase neuroblasts. For all samples, n is noted in the figure.

VRK1 Intensity

Human fibroblasts were stained as described above, imaged on a Zeiss 710 as Z-stacks with equivalent laser power and confocal settings in the same imaging session. Resulting images were analyzed in Imaris (Bitplane) using the Surfaces function to mark nuclear volume. Total intensity sum of the VRK1 channel within the nucleus and nuclear volume were recorded. VRK1 intensity is displayed as intensity sum normalized to volume. One-way ANOVA with multi-comparisons post-test from GraphPad Prism was used to assess significance. Each dot represents one nucleus. Three fields from each cell line were assessed.

DATA AND CODE AVAILABILITY

The dbGaP accession number for all exome sequences reported in this paper and for which informed consent for data sharing in controlled-access databases has been provided under the Baylor College of Medicine Institutional Review Board Protocol Number H-29697. The accession number for the sequences reported in this paper is dbGaP: phs000711.v5.p1. BAB701 was consented under the Baylor College of Medicine Institutional Review Board Protocol Number H-9170 and subjects enrolled through Baylor Genetics Laboratories were consented under the Baylor College of Medicine Institutional Review Board Protocol Number H-41191 which do not allow for data sharing through public repository.